



General linear stability properties of monoclinal shallow waves

Jake Langham ^{1,2,*} and Andrew J. Hogg ¹

¹*School of Mathematics, Fry Building, University of Bristol, Bristol BS8 1UG, United Kingdom*

²*School of Earth Sciences, Wills Memorial Building, University of Bristol, Bristol BS8 1RJ, United Kingdom*



(Received 2 February 2022; accepted 9 May 2022; published 23 May 2022)

We analyze the linear stability of monoclinal traveling waves on a constant incline, which connect uniform flowing regions of differing depths. The classical shallow-water equations are employed, subject to a general resistive drag term. This approach incorporates many flow rheologies into a single setting and enables us to investigate the features that set different systems apart. We derive simple formulas for the onset of linear instability, the corresponding linear growth rates and related properties including the existence of monoclinal waves, development of shocks, and whether instability is initially triggered upstream or downstream of the wave front. Also included within our framework is the presence of shear in the flow velocity profile, which is often neglected in depth-averaged studies. We find that it can significantly modify the threshold for instability. Constant corrections to the governing equations to account for sheared profiles via a “momentum shape factor” act to stabilize traveling waves. More general correction terms are found to have a nontrivial and potentially important quantitative effect on the properties explored. Finally, we have investigated the spatial properties of the dominant (fastest growing) linear modes. We derive equations for their amplitude and frequency and find that both features can become severely amplified near the front of the traveling wave. For flood waves that propagate into a dry downstream region, this amplification is unbounded in the limit of high disturbance frequency. We show that the rate of divergence is a function of the spatial dependence of the wave depth profile at the front, which may be determined straightforwardly from the drag law.

DOI: [10.1103/PhysRevFluids.7.053902](https://doi.org/10.1103/PhysRevFluids.7.053902)

I. INTRODUCTION

Shallow flows of fluid, or other continuous media, are often modeled using a pair of hydrostatic depth-averaged equations describing the conservation of volume and the balance of streamwise momentum. Such models have been employed in many different settings, including classical studies of turbulent open channels [1–4], granular flows [5–9], mud flows [10,11], and gravity currents [12,13]. Specializing a shallow-layer model for each particular case often involves only the selection of a constitutive law for material stresses, which does not affect the mathematical structure of the governing equations. In one spatial dimension, these systems may be written generally in terms of the flow depth $h(x, t)$ and depth-averaged velocity $u(x, t)$, as

$$\frac{\partial h}{\partial t} + \frac{\partial}{\partial x}(hu) = 0, \quad (1a)$$

$$\frac{\partial}{\partial t}(hu) + \frac{\partial}{\partial x}[\beta(h, u)hu^2] + g_{\perp}h \frac{\partial h}{\partial x} = g_{\parallel}h - \frac{\tau(h, u)}{\rho}, \quad (1b)$$

*J.Langham@bristol.ac.uk

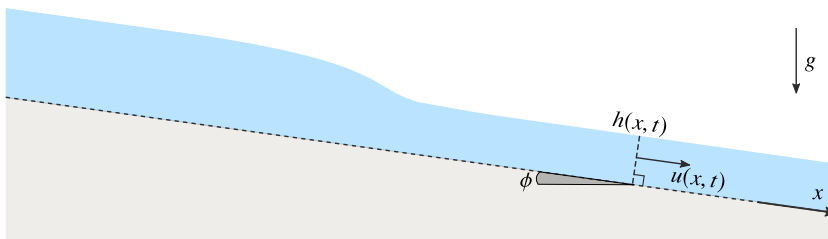


FIG. 1. Diagram of the system under consideration, showing a flow of depth $h(x, t)$ and velocity $u(x, t)$, propagating down a fixed incline at angle ϕ to the horizontal. The profile depicts a typical monoclinal traveling wave solution connecting two uniform flowing layers.

where $g_{\parallel} \equiv g \sin \phi$, $g_{\perp} \equiv g \cos \phi$, i.e., gravitational acceleration resolved parallel and perpendicular to the local slope at angle ϕ to the horizontal (hereafter assumed constant), β is a corrective shape factor that arises during depth-averaging (discussed below), τ models the basal drag on the flowing medium and ρ is the flow density, hereafter assumed constant. By leaving τ as an arbitrary function of the flow variables, many different shallow-layer formulations may be analyzed collectively. This approach was employed previously by Trowbridge [14], who showed in the case of $\beta(h, u) = 1$ that any spatially uniform shallow flow of depth h_0 and velocity u_0 on a constant grade is linearly unstable if

$$\sqrt{g_{\perp} h_0} < \left| \frac{\tau(h_0, u_0) - h_0 \frac{\partial \tau}{\partial h_0}}{\frac{\partial \tau}{\partial u_0}} \right| = h_0 \left| \frac{du_0}{dh_0} \right|. \quad (2)$$

By using this inequality, stability criteria for particular systems may be deduced with ease. The rightmost expression, which is particularly simple to evaluate, is absent from the original analysis [14] and generalizes a stability criterion derived by Craya for turbulent water flows in arbitrary open channels [3]. We include its derivation as a special case of our analysis in Sec. III and note additionally that the inclusion of modulus signs in the inequality permit the assumption of the positivity of its right-hand side to be relaxed [15].

The proliferation of shallow layer models in diverse settings makes the case for conducting general analyses of this kind. Despite this, relatively few studies have adopted a similar viewpoint; see, for example, Refs. [14–17]. The aim of this paper is to extend this program by considering the linear stability properties of steady traveling wave solutions to Eqs. (1a) and (1b), with “monoclinal” depth profiles, which monotonically connect regions with uniform flow depths far upstream and downstream. This class of solutions includes uniform layers as a trivial case and more broadly encompasses both continuous and discontinuous fronts propagating between layers. A sketch of the system, indicating a typical monoclinal wave is given in Fig. 1. Such states are experienced in nature as a surge between two shallow flowing regions of different height. They have been studied widely in the context of turbulent open water [4, 18–21] and more recently, in granular flows [22–26]. The most mathematically extensive results on their stability are available in the former case, where nonlinear stability theorems for monoclinal profiles have been achieved [27, 28]. In the granular setting, the existence and stability of monoclinal traveling were explored for a popular model that includes a small diffusive regularization [24–26]. In addition to these cases, as shall be demonstrated below, monoclinal waves are available as solutions to Eqs. (1a) and (1b) for general drag formulations, provided that the closure permits the existence of steady uniform layers. This includes established models where these states have not been studied in detail.

Our study investigates the existence of traveling waves, their linear stability, and the spatial structure of the corresponding linear modes, within the general setting of Eqs. (1a) and (1b). This consolidates many existing results within a broader framework and provides a perspective through which various properties of different systems may be understood. Moreover, our conclusions may

be simply applied in situations where individual analyses have not been conducted. In particular, for general drag laws we show how to determine whether the monoclinal solution is continuous, discontinuous or even admissible, as a function of downstream flow thickness relative to its upstream thickness, the Froude number of upstream flow (defined shortly in Sec. II), and potentially other parameters that determine the resistance (Sec. II). We compute the linear stability of both continuous and discontinuous waves, determining properties of their associated spectra and deducing a general criterion for instability (Sec. III). The fastest growing linear modes are shown to occur in the asymptotic limit of high wave number (as in the case of uniform layers [14]) and general formulas for their growth rates are given. In certain cases, the frequency and amplitude of these modes are found to be strongly amplified across the wave front. Therefore, we investigate the spatial structure of high-wave number modes and determine when and why amplification occurs using a WKB analysis (Sec. IV). It will be shown that this amplification is particularly extreme for wave fronts that propagate into a region where there is no flowing material. The resulting analysis requires that the WKB approximation is asymptotically matched with separate expansions for the behavior of modes near the wave front and ultimately shows how the drag formulation dictates the rate of amplification with respect to the wave number (Sec. IV B).

Before proceeding, we note that the inclusion of the momentum shape factor β in Eq. (1b) also generalizes our analysis with respect to many prior studies (including Trowbridge’s analysis [14]) of shallow flow linear stability. It is defined as

$$\beta(h, u) = \frac{1}{hu^2} \int_0^h \tilde{u}^2 dz = 1 + \frac{1}{h} \int_0^h \left(\frac{\tilde{u}}{u} - 1 \right)^2 dz, \quad (3)$$

where $\tilde{u} \equiv \tilde{u}(x, z, t)$ denotes the velocity field prior to averaging over the vertical coordinate z , i.e., $hu = \int_0^h \tilde{u} dz$. This parameter represents a correction to the depth-averaging procedure used in deriving shallow-layer formulations. It is evident from Eq. (3) that $\beta(h, u) \geq 1$. Most studies impose $\beta(h, u) = 1$, which formally corresponds to an inviscid model of the flow with no shear in the velocity profile. However, even small discrepancies from unity have been shown to have a marked effect on solutions [29]. We shall demonstrate that it also affects their stability properties. Since β ultimately depends on the particular flow rheology, as well as other observables such as the Reynolds number, we leave it as a general function of h and u in our analysis. While unknown *a priori*, we note that β can be approximated for a given system via Eq. (3), by employing an empirical steady-state representation of \tilde{u} , such as the theory of Ref. [30].

II. EXISTENCE

We begin by postulating the existence of a traveling wave solution to Eqs. (1a) and (1b), propagating at wave speed c_0 and with constant depth H and velocity U in the far-field limit $x \rightarrow -\infty$. Hereafter, we refer to the limits $x \rightarrow -\infty$ and $x \rightarrow \infty$ as the “upstream” and “downstream” directions, respectively. The various quantities in the problem may be nondimensionalized with respect to H , U , g_{\parallel} , and ρ using the transformations

$$x \mapsto xg_{\parallel}/U^2, \quad t \mapsto tg_{\parallel}/U, \quad h \mapsto h/H, \quad u \mapsto u/U, \quad (4a-d)$$

$$c_0 \mapsto c_0/U, \quad \text{and} \quad \tau \mapsto \tau/(\rho g_{\parallel} H). \quad (4e-f)$$

A key control parameter in the forthcoming analysis will be $F = U/(g_{\perp} H)^{1/2}$. This dimensionless combination gives the Froude number of the flow far upstream.

After nondimensionalizing, the governing equations (1a) and (1b) may be rewritten in a more convenient frame by defining the coordinate $\xi = x - c_0 t$, which follows the traveling wave. On making this substitution and simplifying, a compact semilinear matrix equation may be obtained. We first give the resulting system for a general unsteady flow $\mathbf{q}(\xi, t) \equiv [h(\xi, t), u(\xi, t)]^T$ in this

frame:

$$\frac{\partial \mathbf{q}}{\partial t} + J(\mathbf{q}) \frac{\partial \mathbf{q}}{\partial \xi} = \mathbf{G}(\mathbf{q}), \quad (5)$$

where $\mathbf{G}(\mathbf{q}) = (0, 1 - \tau/h)^T$ and $J(\mathbf{q})$ is the Jacobian matrix, given by

$$J(\mathbf{q}) = \begin{pmatrix} u - c_0 & h \\ F^{-2} + B_2 & u - c_0 + B_1 \end{pmatrix}. \quad (6)$$

The terms B_1 and B_2 are placeholders for expressions which vanish when $\beta(h, u) = 1$:

$$B_1 = 2u(\beta - 1) + u^2 \frac{\partial \beta}{\partial u}, \quad \text{and} \quad B_2 = u^2 h^{-1}(\beta - 1) + u^2 \frac{\partial \beta}{\partial h}. \quad (7a,b)$$

The putative traveling wave is a time-independent solution of Eq. (5). Substituting $\mathbf{q} \equiv \mathbf{q}_0(\xi) = [h_0(\xi), u_0(\xi)]^T$ and integrating the first row of the resulting system gives

$$u_0 = c_0 + (1 - c_0)/h_0. \quad (8)$$

Therefore, the steady velocity is a dependent variable, which may in turn be substituted into the second row of Eq. (5), via Eqs. (6) and (7), to obtain

$$\frac{dh_0}{d\xi} = \frac{h_0 - \tau(h_0)}{h_0/F^2 - (c_0 - 1)^2/h_0^2 + (c_0 - 1)B_1/h_0 + h_0B_2}. \quad (9)$$

Since this is an ordinary differential equation in h_0 alone, the only bounded traveling waves that may exist as solutions to Eq. (5) are either everywhere monoclinal, or piecewise monotonic waves separated by discontinuities (as in the case of a roll wave train; see, e.g., Ref. [2]). For continuous nonmonotonic shallow waves to exist, tighter coupling between h_0 and u_0 is needed. This is afforded by the presence of higher-order derivatives (dispersion, diffusion) in some shallow layer formulations; see, e.g., Refs. [4,25,31].

Our focus in this paper is purely monoclinal traveling waves. Moreover, we have assumed finite nonzero depth upstream, with $h_0(\xi), u_0(\xi) \rightarrow 1$ as $\xi \rightarrow -\infty$, by our choice of nondimensionalization. The downstream flow variables necessarily converge to constant values. Therefore, we adopt the notation $h_0(\xi) \rightarrow h_\infty$ and $u_0(\xi) \rightarrow u_\infty$ as $\xi \rightarrow \infty$ and note that the Froude number in this region is given by an appropriate rescaling of the upstream value, $Fu_\infty h_\infty^{-1/2}$. The far-downstream flow determines the speed of the traveling wave, which we deduce from Eq. (8) to be

$$c_0 = \frac{1 - h_\infty u_\infty}{1 - h_\infty}. \quad (10)$$

Since u_0 depends on h_0 and c_0 only, we note that $c_0 \equiv c_0(h_\infty)$, with $c_0(0) = 1$ in the special case $h_\infty = 0$, where a wave front connects to a dry downstream region, referred to hereafter as a ‘‘flood wave.’’ We shall focus our analysis primarily on waves with $h_\infty \leq 1$, since this is the most typically observed and studied case.

To illustrate our results and investigate the effect of drag, we shall refer to various closures for the function τ throughout the paper. By considering Eq. (9) in the uniform flow regime far upstream, we see that $\tau(1, 1) = 1$. This often allows at least one empirical parameter to be scaled out from a given closure formula, leading to simple functional forms for τ . For example, turbulent fluid (Chézy) drag is given by $\tau(h, u) = u^2$, while the drag on a viscously dominated fluid is $\tau(h, u) = u/h$. A number of results will be explored using the following rheology employed in the modeling of granular media [32–34]:

$$\tau(h, u) = \frac{\mu(h, u)h}{\mu(1, 1)}, \quad \text{where} \quad \mu(h, u) = \mu_1 + \frac{\mu_2 - \mu_1}{1 + \zeta h^{3/2}/(Fu)}, \quad (11)$$

with μ_1, μ_2 , and ζ empirically determined constants. Although other possible parametrizations exist to describe granular flows via specification of μ (examples include Refs. [5,35,36]), our aim herein

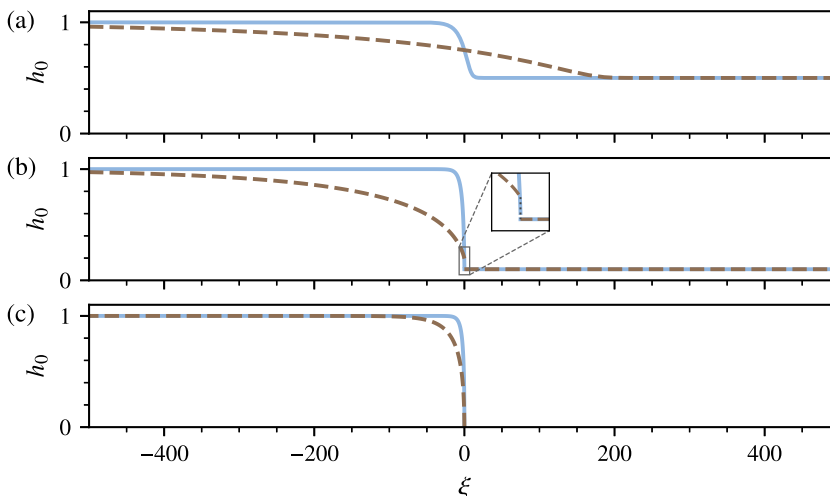


FIG. 2. Example traveling wave solutions satisfying Eq. (9) with $\beta = 1$ and $F = 0.5$, for Chézy drag (solid blue) and granular drag (dashed brown). The separate panels show connections from $h_0 = 1$ upstream to different downstream depths: (a) continuous monoclinal waves with $h_\infty = 0.5$, (b) shock profiles with $h_\infty = 0.1$, and (c) flood wave solutions with $h_\infty = 0$.

is not to analyze the selection of individual closures. Therefore, we simply fix the illustrative values $\mu_1 = 0.1$, $\mu_2 = 0.4$, $\zeta = 10$ and refer to Eq. (11) as “granular drag” throughout the paper.

On specifying F , h_∞ , and τ , Eq. (9) may be integrated to obtain a monoclinal wave solution. In some cases, $dh_0/d\xi$ is singular, in which case a shock with velocity c_0 must be fitted at the singular point to complete the wave profile. Translational invariance permits us to locate this at $\xi = 0$. Discontinuous solutions to Eq. (5), must satisfy the appropriate Rankine-Hugoniot conditions across a shock. These ensure conservation of mass and momentum fluxes across $\xi = 0$ and are straightforwardly obtained to be

$$[h(u - c_0)]_{\pm}^{\pm} = 0 \quad \text{and} \quad \left[hu(\beta u - c_0) + \frac{h^2}{2F^2} \right]_{\pm}^{\pm} = 0, \quad (12a,b)$$

where $[f(\xi)]_{\pm}^{\pm} \equiv f(0^+) - f(0^-)$. The downstream traveling wave is then given by $h_0(\xi) = h_\infty$, $u_0(\xi) = u_\infty$ for $\xi > 0$, and at $\xi = 0^-$ we apply Eq. (12) to deduce that the height of the shock is

$$h_0(0^-) = \frac{h_\infty}{2} \left\{ \left[\frac{8\beta F^2 (c_0 - 1)^2}{h_\infty^3} + \left(1 + \frac{2F^2 c_0^2 (\beta - 1)}{h_\infty} \right)^{2/3} \right]^{1/2} - 1 \right\} - (\beta - 1)F^2 c_0^2. \quad (13)$$

Note that, since this equation does not bound the magnitude of $h_0(0^-)$, it is possible for “monoclinal” shock solutions to be strictly increasing for $\xi < 0$, before abruptly dropping to some $h_\infty < 1$ across the shock. However, upturned shock waves of this sort are not necessarily stable. We discuss the stability of such solutions in general later, in Sec. III B.

Some example traveling waves are demonstrated in Fig. 2. Across Figs. 2(a)–2(c), the solutions plotted connect to progressively lower downstream levels. As h_∞ decreases from unity, continuous monoclinal waves develop a shock before ultimately becoming flood waves when $h_\infty = 0$. To understand the regimes of Fig. 2 generally, it is informative to consider the two characteristic curves $\lambda_1(h, u)$, $\lambda_2(h, u)$ of the underlying system Eq. (5), given by the eigenvalues of the Jacobian defined

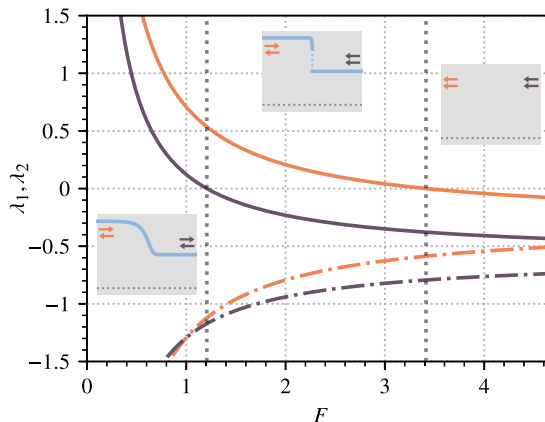


FIG. 3. Dependence of far-field characteristics λ_1 (solid) and λ_2 (dash-dot) on F , for Chézy drag monoclinal waves with $h_\infty = 0.5$ and $\beta = 1$. Upstream values are plotted with orange curves, downstream with purple curves. The inlaid diagrams show the directions of propagation of the characteristics in the three distinct solution regimes given by inequalities (16) to (18) (continuous waves, shock waves, no solution). These regimes are separated by vertical dotted lines. The wave profiles plotted in the leftmost and middle diagrams are $h_0(\xi)$ at $F = 0.6$ and 1.8 , respectively, within the interval $\xi \in [-50, 50]$.

in Eq. (6). We compute them to be

$$\lambda_1(h, u) = u - c_0 + \frac{B_1}{2} - \sqrt{\frac{h}{F^2} + hB_2 + \left(\frac{B_1}{2}\right)^2}, \quad (14a)$$

$$\lambda_2(h, u) = u - c_0 + \frac{B_1}{2} + \sqrt{\frac{h}{F^2} + hB_2 + \left(\frac{B_1}{2}\right)^2}. \quad (14b)$$

Note that if $B_2 < 0$, it is possible for the characteristics to be complex-valued, leading to elliptic equations that cannot be well posed as initial value problems. Therefore, we assume that λ_1 and λ_2 are distinct and real-valued, so that Eq. (5) is strictly hyperbolic, as in the often used case with $\beta = 1$ (i.e., $B_1 = B_2 = 0$). The consequences of loss of strict hyperbolicity are addressed further in Sec. III.

The signs of $\lambda_1(h, u)$ and $\lambda_2(h, u)$ in the upstream and downstream limits $\xi \rightarrow \pm\infty$ dictate suitable boundary conditions for the problem and, ultimately, whether the two far-field regions must be connected via a shock. We illustrate this with Fig. 3, in which the values of the upstream and downstream characteristics are plotted (in orange and purple respectively) for Chézy drag and waves with $h_\infty = 0.5$ and $\beta = 1$. In the leftmost regime ($F \lesssim 1.2$), the characteristics possess opposite signs both upstream and downstream, and continuous monoclinal solutions exist that connect the far-field regions. For greater values of F , λ_1 changes sign in the far downstream. Consequently, both characteristics propagate into the domain from the boundary at $\xi = +\infty$, and solutions contain a shock (across which λ_1 changes sign) connecting the supercritical downstream flow to the incoming wave. When $F \gtrsim 3.4$, λ_1 becomes negative in the $\xi \rightarrow -\infty$ limit also. The governing system can no longer be posed with upstream boundary conditions in this regime, so monoclinal solutions cease to exist.

We shall demonstrate that this picture does not qualitatively depend on the drag law or on the shape factor. To determine the nature of the far-field characteristics in general, we split our analysis into multiple cases, since β is an unknown parameter, meaning that we cannot be sure of the sign of $u_0 - c_0 + B_1/2$ in either region. Furthermore, for the remainder of this section only, we make two simplifying assumptions. First, we assume that $u_\infty(h_\infty)$ is a monotonically increasing

function. This is true for most physical drag formulations, including all examples given in this paper. Therefore, $0 \leq u_\infty \leq 1$ when $0 \leq h_\infty \leq 1$ and using Eq. (10), we conclude that $c_0 \geq 1$. Second, we assume that the derivatives $\partial\beta/\partial h$ and $\partial\beta/\partial u$ vanish, or are negligible, so that $B_1 = 2u(\beta - 1)$ and $B_2 = (\beta - 1)u^2/h$. Restricting these degrees of freedom in this way permits us to find relatively succinct conditions for the different solution regimes of the problem.

First, we turn our attention to the upstream boundary, $\xi \rightarrow -\infty$, where $u_0 - c_0 + B_1/2 = \beta - c_0$. Suppose that $\beta - c_0 < 0$. Then $\lambda_1(1, 1) < 0$. Moreover, $\lambda_2(1, 1) < 0$, when $F^2 > [(c_0 - \beta)^2 - \beta(\beta - 1)]^{-1}$ is satisfied. In this case, both characteristics propagate out of the domain, and there are no admissible boundary conditions. For smaller values of F , λ_2 becomes positive, so $h_0 \rightarrow 1$ may be imposed at the upstream boundary. Suppose instead that $\beta - c_0 > 0$. This is the case for waves approaching the flood wave limit, $h_\infty \rightarrow 0$ (where $c_0 \rightarrow 1$). Then $\lambda_2(1, 1) > 0$. Furthermore, we can deduce that $\lambda_1(1, 1) < 0$. To see this, suppose otherwise. Then (recalling that $c_0 > 1$) the following chain of inequalities would hold:

$$(\beta - 1)^2 > (\beta - c_0)^2 > F^{-2} + \beta(\beta - 1) > \beta(\beta - 1), \quad (15)$$

which contradicts $\beta > 1$.

Similar arguments apply in the case of the downstream region $\xi \rightarrow \infty$, where we deduce that $\lambda_1(h_\infty, u_\infty)$ and $\lambda_2(h_\infty, u_\infty)$ possess opposite sign if and only if $F^2 > h_\infty[(c_0 - \beta u_\infty)^2 - \beta(\beta - 1)u_\infty^2]^{-1}$ (otherwise both are negative). Therefore, in summary, at both ends of the domain, the characteristics have opposite signs if and only if

$$0 < F < \left(\frac{h_\infty}{(c_0 - \beta u_\infty)^2 - \beta(\beta - 1)u_\infty^2} \right)^{1/2}. \quad (16)$$

(Depending on the sign of $\beta - c_0$, this inequality is satisfied automatically in some situations.) In this case, we anticipate a continuous monoclinal wave connecting from the boundary condition $h = 1$ at $\xi = -\infty$, through to $h = h_\infty < 1$ at $\xi = +\infty$.

If instead, we have

$$\left(\frac{h_\infty}{(c_0 - \beta u_\infty)^2 - \beta(\beta - 1)u_\infty^2} \right)^{1/2} < F < \left(\frac{1}{(c_0 - \beta)^2 - \beta(\beta - 1)} \right)^{1/2}, \quad (17)$$

then both characteristics at $\xi \rightarrow +\infty$ propagate into the domain. The uniform layer in this region is therefore supercritical and connects to the upstream flow via a discontinuity.

Finally, if

$$F > \left(\frac{1}{(c_0 - \beta)^2 - \beta(\beta - 1)} \right)^{1/2}, \quad (18)$$

then the characteristics propagate out of the domain at the upstream boundary and there are no admissible boundary conditions there. Note that, when $\beta = 1$, this inequality cannot be satisfied in the flood wave case, because $c_0 = 1$. More generally, we can deduce from inequality (18) that monoclinal traveling wave solutions exist for arbitrary F , when the wave speed c_0 satisfies

$$1 \leq c_0 \leq \beta + \sqrt{\beta(\beta - 1)}. \quad (19)$$

Since $c_0 \equiv c_0(h_\infty)$, this should be interpreted as an interval of shallow downstream flow depths for which solutions always exist.

In Fig. 4 we indicate the solution regimes for both [Fig. 4(a)] Chézy drag and [Fig. 4(b)] granular drag. The standard case $\beta = 1$ is marked with solid curves, delineating the boundaries of the inequalities (16) and (18). Increasing the vertical shear ($\beta > 1$) broadens the regions of existence for both continuous and discontinuous solutions with $h_\infty < 1$. For completeness, we continue the curves into the $h_\infty > 1$ parameter region. In this case, the requirements for the downstream layer to connect to the upstream are reversed, meaning that continuous monoclinal waves exist at higher F than shock solutions. For uniform layers $h_\infty = 1$, there is no distinction between shocks and

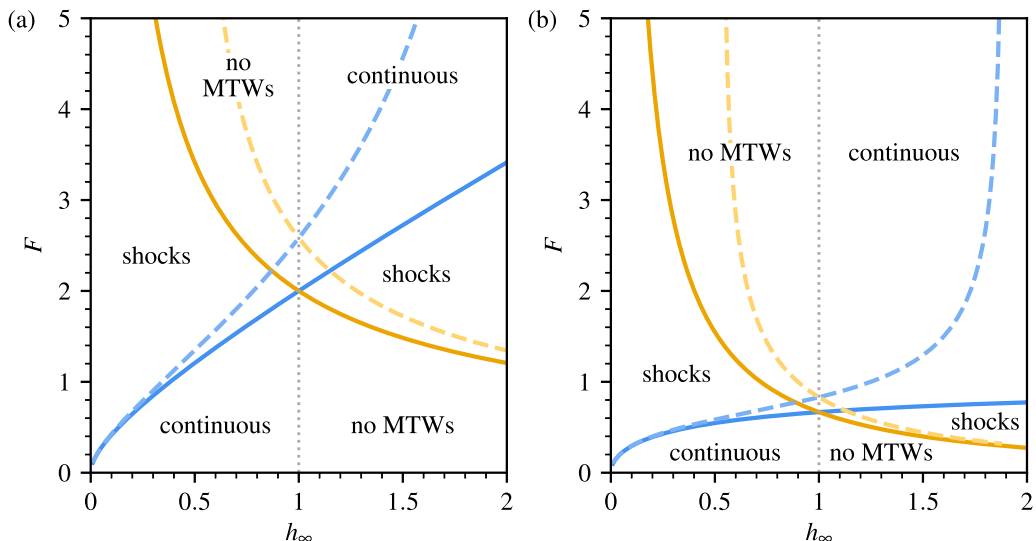


FIG. 4. Existence of monoclinal traveling waves (MTWs) in the (h_∞, F) plane for (a) Chézy drag and (b) granular drag. The blue and orange lines denote the boundaries of the labeled regimes, given by the inequalities (16) and (18), respectively. Solid lines show the $\beta = 1$ case and dashed lines show the $\beta = 1.05$ case in panel (a) and $\beta = 1.2$ in panel (b).

continuous solutions, which exist for all F . Consequently, the regime boundaries merge. Note that the crossing point occurs at exactly the critical F marking the onset of instability in a uniform layer (for example, $F = 2$ for Chézy drag [1] and $F = 2/3$ for granular drag [6], when $\beta = 1$). In Sec. III we will show why this must be true in general.

III. LINEAR STABILITY

To analyze the response of the traveling wave to perturbations, we introduce a small amplitude disturbance that develops linearly with arbitrary complex growth rate σ . If the wave features a discontinuity, then we must allow for the corresponding shock location to be perturbed also. Equivalently, we choose to keep it pinned to $\xi = 0$ and perturb the underlying coordinate frame. Therefore, we write

$$\mathbf{q}(\xi, t) = \mathbf{q}_0(\xi) + \varepsilon \mathbf{q}_1(\xi) e^{\sigma t} + \dots, \quad (20a)$$

$$\xi = \xi_0 + \varepsilon \xi_1 e^{\sigma t} + \dots, \quad (20b)$$

where $\xi_0 = x - c_0 t$ and the unknowns \mathbf{q}_1, ξ_1 are $O(1)$ with respect to the small nonzero parameter ε . The corresponding perturbed shock velocity is $c_0 + \varepsilon c_1 e^{\sigma t}$, with $c_1 = -\sigma \xi_1$. Linearizing Eq. (5) with respect to this expansion and simplifying using the $O(1)$ expression, we obtain the following compact equation governing the perturbation:

$$\sigma \hat{\mathbf{q}}_1 + \mathbf{J}(\mathbf{q}_0) \hat{\mathbf{q}}_1' + \mathbf{N}(\mathbf{q}_0) \hat{\mathbf{q}}_1 = \mathbf{0}, \quad (21)$$

where, using primes to denote total derivatives with respect to ξ , we have defined a transformed perturbation vector

$$\hat{\mathbf{q}}_1 = (\hat{h}_1, \hat{u}_1)^T \equiv \mathbf{q}_1 + \xi_1 \mathbf{q}'_0 \quad (22)$$

and a matrix $\mathbf{N}(\mathbf{q}_0)$ whose entries N_{ij} are given by

$$N_{ij} = \frac{\partial J(\mathbf{q}_0)_{ik}}{\partial q_j} (\mathbf{q}'_0)_k - \frac{\partial \mathbf{G}(\mathbf{q}_0)_i}{\partial q_j}. \quad (23)$$

The variable transformation in Eq. (22) is typical of studies in similar settings (e.g., Ref. [27]) and allows the linear equations to be written in a form that is independent of whether shocks are present ($\xi_1 \neq 0$). The only material difference between these two cases is that the evolution of any shock must also obey the jump conditions of Eq. (12) at $\xi = 0$, which after perturbing become

$$[h_1(u_0 - c_0) + h_0(u_1 - c_1)]^+ = 0, \quad (24a)$$

$$\left[h_0 u_0 (\beta u_1 - c_1) + (h_1 u_0 + h_0 u_1) (\beta u_0 - c_0) + \frac{h_0 h_1}{F^2} \right]^+ = 0, \quad (24b)$$

to linear order.

In both far-field limits $\xi \rightarrow \pm\infty$, the base solution $\mathbf{q}_0(\xi)$ is spatially constant. Consequently, Eq. (21) may be solved directly in these regimes in terms of normal modes of complex wave number k_- upstream and k_+ downstream. Therefore, we seek eigenmodes of Eq. (21) subject to the boundary conditions

$$\hat{\mathbf{q}}_1(\xi) \rightarrow \exp(ik_{\pm}\xi)\hat{\mathbf{q}}_{\pm} \quad \text{as } \xi \rightarrow \pm\infty, \quad (25)$$

where $\hat{\mathbf{q}}_-$ and $\hat{\mathbf{q}}_+$ are *a priori* unknown constant vectors. Then we may eliminate $\hat{\mathbf{q}}_1$ from Eq. (21) in either of the far-field limits, to obtain the dispersion relations

$$\eta_{\pm}(\sigma + i\lambda_{1\pm}k_{\pm})(\sigma + i\lambda_{2\pm}k_{\pm}) + \sigma + ia_{\pm}k_{\pm} = 0, \quad (26)$$

where (using a colon to denote the Frobenius inner product of matrices)

$$\eta_{\pm} = \text{tr}(N_{\pm})^{-1} \quad \text{and} \quad a_{\pm} = \eta_{\pm} \det(J_{\pm})(J_{\pm}^{-1})^T : N_{\pm}, \quad (27a,b)$$

with $\lambda_{1\pm} \equiv \lim_{\xi \rightarrow \pm\infty} \lambda_1$, $\lambda_{2\pm} \equiv \lim_{\xi \rightarrow \pm\infty} \lambda_2$, $J_{\pm} \equiv \lim_{\xi \rightarrow \pm\infty} J(\mathbf{q}_0)$, and $N_{\pm} \equiv \lim_{\xi \rightarrow \pm\infty} N(\mathbf{q}_0)$. In deriving Eq. (26), we made use of the fact that $\det(N_{\pm}) = 0$, which follows from the definition of \mathbf{G} and the fact that the first term on the right-hand side of Eq. (23) vanishes as $|\xi| \rightarrow \infty$. The relation holds for arbitrary J in Eq. (5). It will be useful for later discussion to appreciate that terms of the form $\sigma + ick$ are the algebraic equivalent of the operator $\partial/\partial t + c\partial/\partial \xi$ under the Laplace and Fourier transforms implicitly employed in Eqs. (20a) and (25). Hence, Eq. (26) factorizes the linear dynamics of disturbances in terms of wave transport operators with velocities $\lambda_{1\pm}$, $\lambda_{2\pm}$ and a_{\pm} .

For any σ , there are two solutions of Eq. (26) for both k_- and k_+ . The signs of $\text{Im}(k_-)$ and $\text{Im}(k_+)$ dictate whether the corresponding eigenmode $\hat{\mathbf{q}}_1$ grows or decays in each far-field limit. Equivalently, they determine the stability (with respect to spatial integration) of the fixed point $\hat{\mathbf{q}}_1(\xi) = (0, 0)^T$ of Eq. (21) far upstream and downstream. Any linear mode must be bounded in order to be counted as a small perturbation. For such a mode to exist with a given σ , at least one solution of Eq. (26) for k_- must have $\text{Im}(k_-) \leq 0$ and likewise, at least one k_+ must satisfy $\text{Im}(k_+) \geq 0$. Note also that $\text{Re}(k_-)$ and $\text{Re}(k_+)$ differ in general, indicating that the spatial modulation of $\hat{\mathbf{q}}_1$ varies across the traveling wave front. Examples of modes with this interesting property are given in Fig. 5.

The constraints that Eq. (26) places on the linear problem are illustrated in Fig. 5(a), which depicts the spectrum for a monoclinal wave subject to granular drag, with $F = 0.5$ and $h_{\infty} = 0.5$. We find that the essential features of this figure are typical of other drag rules (e.g., Chézy and viscous drag). Regions of the plot are labeled according to the signs of $\text{Im}(k_-)$ and $\text{Im}(k_+)$. In region I, both k_- solutions of Eq. (26) have $\text{Im}(k_-) < 0$ and both k_+ solutions have $\text{Im}(k_+) > 0$. That is, $(0, 0)^T$ is a repeller of Eq. (21) at $\xi = -\infty$ and an attractor at $\xi = \infty$. Crossing from region I to region II, there is a sign change in one of the branches of $\text{Im}(k_+)$, indicated by the bounding $\text{Im}(k_+) = 0$ curve (dashed blue). This leaves a saddle point at $\xi = \infty$. For any σ in either I and II, eigenmodes may be obtained by integrating Eq. (21) backwards in space from $\xi = \infty$ to $\xi = -\infty$. Within region II, bounded solutions to Eq. (21) must leave $\xi = \infty$ along the stable manifold of the far-field fixed point, so the eigenspace is unidimensional in this case. The union of regions I and II forms the essential spectrum, whose modes are continuously parametrized by σ . Region III designates the case where both upstream and downstream limits are saddle points. In order for

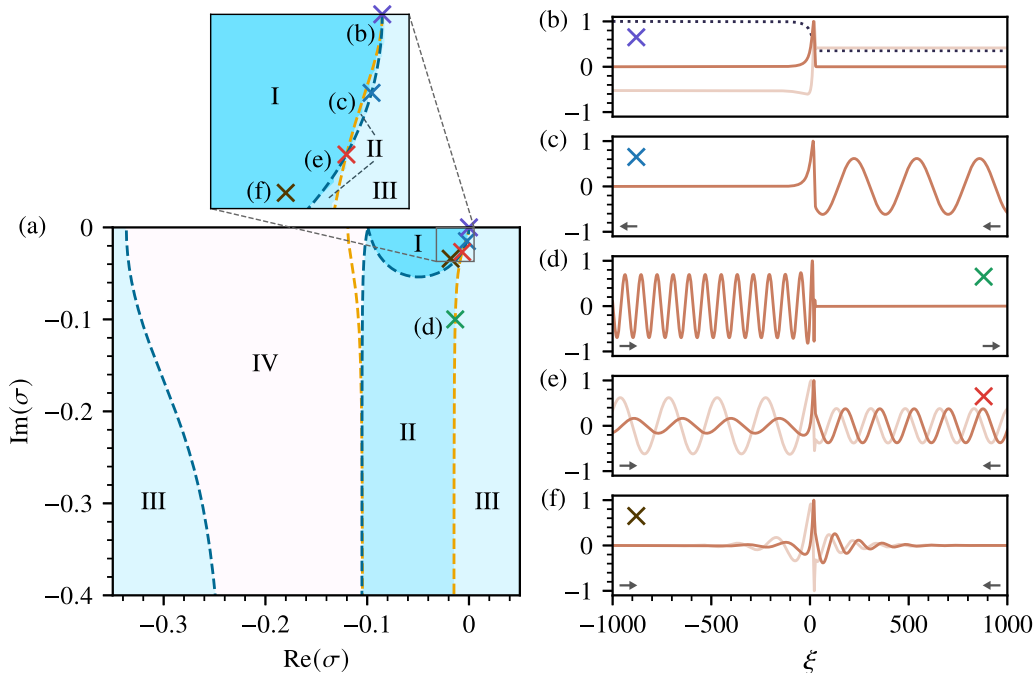


FIG. 5. Spectrum diagram for the continuous monochloral wave with $F = 0.5$, $h_\infty = 0.5$ and the granular drag law given in Eq. (11). Different regions of the spectrum are indicated in (a), labeled I–IV according to the signs of the far-field spatial decay rates $\text{Im}(k_-)$ and $\text{Im}(k_+)$. Details of this labeling are given in the main text. The critical lines $\text{Im}(k_-) = 0$ and $\text{Im}(k_+) = 0$ are plotted with yellow and blue dashes, respectively. Since the spectrum is symmetric about $\text{Im}(\sigma) = 0$, since $\exp(ik\xi + \sigma t)$ is invariant with respect to the transformation $\sigma \mapsto \bar{\sigma}$, $k \mapsto -\bar{k}$ (where the overbar denotes complex conjugation), we have omitted the upper half-plane. Regions I and II make up the essential spectrum, from which we show a selection of example modes, plotting $u_1(\xi)$ with solid curves in panels (b)–(f). Arrows indicate the direction of the perturbation velocities in the far field. In (b) we also plot the base solution $u_0(\xi)$ (dotted). The exact growth rates of the computed modes, as indicated by crosses in panel (a), are $\sigma =$ (b) 0, (c) $-0.002 - 0.01495i$, (d) $-0.0135 - 0.1i$, (e) $-0.00667881 - 0.0267i$, and (f) $-0.018 - 0.034i$. Where two modes exist (b, e, f), the plotted curves are first orthogonalized with respect to the inner product defined by $\langle f, g \rangle = \int_{-\infty}^{\infty} f(\xi)g(\xi)e^{-\xi/100} d\xi$.

modes to exist in this region, the unstable manifold of Eq. (21) at $\xi \rightarrow -\infty$ must form a heteroclinic connection with the stable manifold at $\xi \rightarrow \infty$. Such connections are not robust to perturbations of σ and any modes in region II are thus isolated, forming the point spectrum of the linear operator. Sophisticated numerical methods exist for assessing the existence of these discrete modes [37]. However, they necessitate the specification of a particular β and τ . Therefore, we must regrettably limit our scope to considering the essential spectrum only. (See Sec. V for further discussion.) In the current example of granular waves, we briefly searched for modes in the unstable part of region II various F and h_∞ and found none. Completing the qualitative description of Fig. 5(a), region IV indicates the regime where there can be no admissible eigenmodes, since either $\xi = -\infty$ is an attractor or $\xi = \infty$ is a repeller (or both).

We note that the essential spectrum of our example wave does not cross $\text{Re}(\sigma) = 0$ and is therefore linearly stable. In Figs. 5(b)–5(f) we plot a selection of modes from this region; their locations in the spectrum are as indicated in Fig. 5(a). (The velocity perturbation u_1 is plotted, but h_1 is similar in each case.) First, in Fig. 5(b), which also includes the base solution $u_0(\xi)$ for reference (dotted), we plot the two neutral stability modes with $\sigma = 0$. The darker curve is (the velocity field

of) the mode $(h_1, u_1) = (-h'_0, -u'_0)$, which arises due to invariance of the traveling wave to shifts along ξ . Its lighter counterpart corresponds to neutral perturbations along the family of steady wave solutions that are parametrized by the downstream depth h_∞ . Both curves feature a sharp peak in the neighborhood of $\xi = 0$ where the wave profile is steepest. The mode in Fig. 5(c) lies close to the origin on the curve $\text{Im}(k_+) = 0$ and is consequently undamped in the downstream regime. In the upslope direction, it decays rapidly towards a saddle point at $\xi = -\infty$. At the wave front, the mode features dramatic amplification, likely inherited from the nearby neutral modes. In Fig. 5(d) we plot a mode on the curve $\text{Im}(k_-) = 0$, which is conversely undamped in the upstream far field and decays rapidly as $\xi \rightarrow \infty$. For a mode to be undamped in both directions it must lie on one of the discrete set of intersection points of the critical curves. We isolate such a point in Fig. 5(e) and note that the corresponding modes are formed from the convergence of two distinct wave numbers. Last, in Fig. 5(f) we include a pair of modes in the interior of the essential spectrum, which decay in both upstream and downstream directions. For each mode plot, we have included arrows showing the propagation directions associated with the dominant perturbation velocities $-\text{Im}(\sigma)/\text{Re}(k_\pm)$ in the far-field regimes. (From the two linear independent components of each mode, either we use either the least spatially damped wave number, or, in the case of saddle points, we take the component that remains bounded in the relevant far-field limit.) We observe that the purely harmonic parts of modes in Figs. 5(c)–5(e) are directed towards the wave front in each case, regardless of whether these undamped regions lie upstream or downstream.

In Fig. 6 we demonstrate the changes to the spectrum of the traveling wave as F is increased from its value of 0.5 in Fig. 5, with $h_\infty = 0.5$ remaining fixed. Increasing F to 0.55 [Fig. 6(a)] leaves the wave slightly above the threshold for shock formation [see Fig. 4(b)]. The resulting spectrum is qualitatively very different from the case of a continuous monoclinal wave. This is because crossing the threshold between continuous and discontinuous solutions induces a sign change in one of the branches of $\text{Im}(k_+)$, thereby altering the stability of the fixed point at $\xi = \infty$. For example, region I in Fig. 5 is labeled II in Fig. 6(a), since the attractor at $\xi = \infty$ becomes a saddle point when solutions possess a shock. The sign change in $\text{Im}(k_+)$ occurs precisely because of the sign change in λ_{2+} that we argued in Sec. II necessitates shock development. When λ_{2+} passes through zero, the leading term in Eq. (26) vanishes and one branch of $\text{Im}(k_+)$ passes through a singularity associated with this degeneracy. We note that this also causes a topological change in the $\text{Im}(k_+) = 0$ curve, whose branch near the origin no longer forms a complete loop. Within the region enclosed between the two branches of this curve (dashed blue), the $\xi \rightarrow \infty$ point is a saddle, while to the left and right it is respectively an attractor and a repeller. The stability of the $\xi \rightarrow -\infty$ point remains qualitatively equivalent to the Fig. 5 case. Continuously parametrized modes exist in region II, which is disconnected and stable. Furthermore, in this case we may also consider modes which are identically zero in either the upstream ($\xi < 0$) or downstream ($\xi > 0$) direction. In particular, we find that upstream disturbances connecting to an unperturbed downstream exist as bounded solutions to Eq. (21) everywhere enclosed within the two branches of $\text{Im}(k_-) = 0$ (dashed yellow). The light blue hatched region denotes a region of the spectrum where only these “upstream” modes exist. We include a plot of one of these modes in Fig. 6(b) alongside the underlying traveling shock profile and note that the mode amplitude is significantly amplified at the discontinuous wave front.

Figure 6(c) shows the spectrum for an unstable traveling wave, with $F = 0.8$ and $h_\infty = 0.5$. In this case we see that the regions remain qualitatively similar to those in Fig. 6(a). It is the upstream modes only that cross $\text{Re}(\sigma) = 0$, becoming unstable, with the maximum growth rate attained for large values of $|\text{Im}(\sigma)|$, i.e., the most rapidly propagating disturbances. An example of such a mode is plotted in Fig. 6(d), at $\text{Im}(\sigma) = -0.2$, matching the mode plotted in Fig. 6(b). Modes with nonzero downstream perturbations are all stable at this value of F . Following the continuation of our stability analysis below, we shall show that this observation is not a generic property of these systems. Whether the upstream regime is more vulnerable to instability than the downstream or vice versa depends on the particular drag closure.

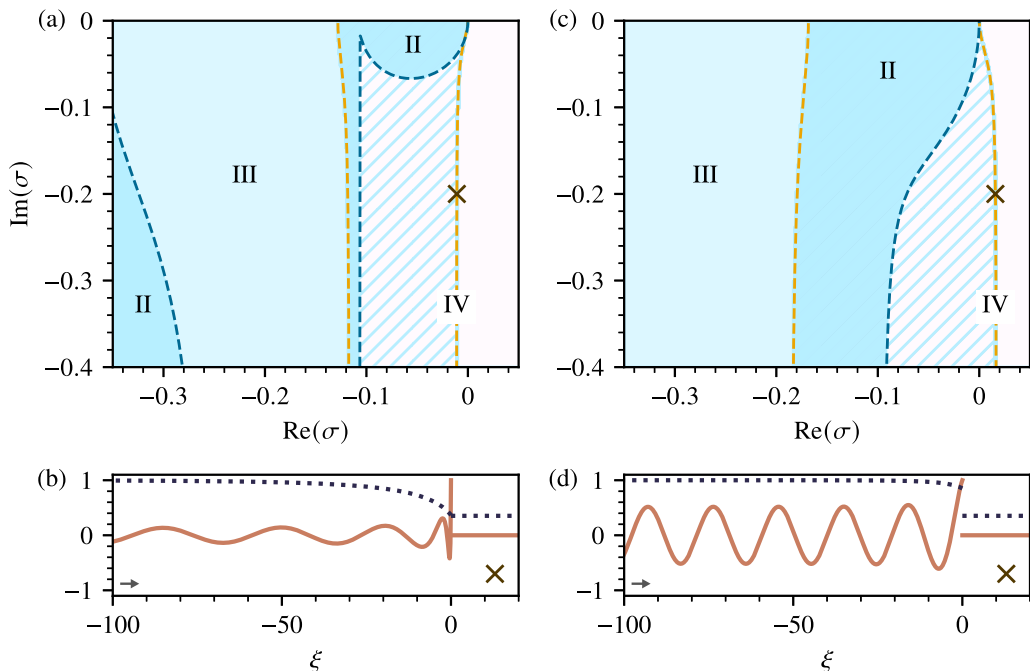


FIG. 6. Spectra for discontinuous traveling waves with granular drag and $h_\infty = 0.5$. Panel (a) shows the case $F = 0.55$, close to the boundary of and within the regime of discontinuous states. The labeling and color scheme match the conventions of Fig. 5. An example mode is plotted in (b), which shows the $u_1(\xi)$ field of the mode at the location labeled with a cross in (a), $\sigma = -0.0109 - 0.2i$ (solid). The velocity of the base traveling solution, $u_0(\xi)$, is also shown (dotted). Panel (c) plots the spectrum of an unstable case with $F = 0.8$. In (d) we plot the $u_1(\xi)$ field of the undamped unstable mode whose imaginary growth rate matches the example in (b), in this case located at the cross in (c), $\sigma = 0.0159 - 0.2i$ (solid). The velocity of the base solution is also given (dotted). In both panels (b) and (d), arrows indicate the direction of the perturbation velocity far upstream.

A. Deriving a general stability criterion

The curves $\text{Im}(k_-) = 0$ and $\text{Im}(k_+) = 0$ where modes are undamped in the far field necessarily dictate the boundary of the essential spectrum. Therefore, to assess the stability of traveling waves (with respect to continuously parametrized modes) in generality, we must determine when these curves cross $\text{Re}(\sigma) = 0$. Therefore, we suppose that $k_\pm \in \mathbb{R}$ for the remainder of this section and write $\sigma = \sigma_r + i\sigma_i$, with $\sigma_r, \sigma_i \in \mathbb{R}$. On separating out the real and imaginary parts of Eq. (26), we obtain

$$\sigma_r^2 - \sigma_i^2 - \sigma_i(\lambda_{1\pm} + \lambda_{2\pm}) - k_\pm^2 \lambda_{1\pm} \lambda_{2\pm} + \sigma_r \eta_\pm^{-1} = 0, \quad (28a)$$

$$\eta_\pm \sigma_r [2\sigma_i + (\lambda_{1\pm} + \lambda_{2\pm})k_\pm] + a_\pm k_\pm + \sigma_i = 0. \quad (28b)$$

When $k_\pm = 0$, the solutions of these equations are $\sigma = 0, -1/\eta_\pm$. The first of these corresponds to the aforementioned pair of neutral stability modes, while the second corresponds to global perturbations whose stability depends on $\text{sgn}(\eta_\pm)$. We shall suppose that $\eta_\pm > 0$, which is the practical case of interest in applications, where solutions are stable to spatially uniform modes.

Eliminating σ_i and simplifying leads to the following expression:

$$k_{\pm}^2 = \frac{\sigma_r(\eta_{\pm}\sigma_r + 1)(2\eta_{\pm}\sigma_r + 1)^2}{\eta_{\pm}^3(s_1 - \sigma_r)(\sigma_r - s_2)(\lambda_{2\pm} - \lambda_{1\pm})^2}, \quad (29a-c)$$

$$\text{where } s_1 \equiv \frac{a_{\pm} - \lambda_{2\pm}}{\eta_{\pm}(\lambda_{2\pm} - \lambda_{1\pm})}, \quad s_2 \equiv \frac{\lambda_{1\pm} - a_{\pm}}{\eta_{\pm}(\lambda_{2\pm} - \lambda_{1\pm})}.$$

Therefore, when $|k_{\pm}| \gg 1$, we find that the two branches of σ_r asymptotically approach the limiting values s_1 and s_2 . [For example, in Fig. 5(a) these asymptotes are at $\sigma_r \approx -0.104, -0.0149$ for $\xi \rightarrow -\infty$ and $\sigma_r \approx -0.231, -0.105$ for $\xi \rightarrow \infty$, which match values computed for s_1 and s_2 in the respective far-field regions.] Moreover, for general k_{\pm} , Eq. (29) may be differentiated to obtain a formula for $\partial\sigma_r/\partial k_{\pm}$, which is zero if and only if $k_{\pm} = 0$ or $\sigma_r = s_1, s_2$. Hence, both branches of $\sigma_r(k_{\pm})$ are even functions which are monotonic with respect to $|k_{\pm}|$ and must be bounded by their values in the zero ($\sigma_r = -\eta_{\pm}^{-1}, 0$) and high wave number ($\sigma_r = s_1, s_2$) regimes.

Since the growth rate is always stable for $k_{\pm} = 0$, we conclude that $s_1 \leq 0$ and $s_2 \leq 0$ for a linearly stable traveling wave,

$$\lambda_{1\pm} \leq a_{\pm} \leq \lambda_{2\pm}, \quad (30)$$

in both far-field limits, with the onset of instability occurring at potentially either of the critical cases $a_{\pm} = \lambda_{1\pm}$ or $a_{\pm} = \lambda_{2\pm}$. This recovers the results of Whitham [4,38], who noted that linear instabilities occur in systems of conservation laws when the propagation velocity of the bulk disturbance intersects with the characteristics. As noted earlier, the quantities a_{-} and a_{+} may be identified as far-field wave velocities. They correspond to a reduced description of the linear dynamics that omits the propagation of high frequencies, which are carried by the leftmost term of Eq. (26) at the characteristic velocities. Instabilities first arise when the wave speeds of these low- (a_{\pm}) and high-frequency ($\lambda_{1\pm}$ and $\lambda_{2\pm}$) descriptions intersect (in either far field).

Turning attention toward our particular application, we may consult Eqs. (6), (23), and (27a,b) and compute

$$\eta_{\pm} = \lim_{\xi \rightarrow \pm\infty} f_u^{-1}, \quad a_{\pm} = \lim_{\xi \rightarrow \pm\infty} (u_0 - c_0 - h_0 f_h / f_u), \quad (31a,b)$$

where we define the following terms, which arise from linearization of the drag function:

$$f_h \equiv \frac{1}{h_0} \left(\frac{\partial \tau}{\partial h} \Big|_{q=q_0} - \frac{\tau(q_0)}{h_0} \right), \quad f_u \equiv \frac{1}{h_0} \frac{\partial \tau}{\partial u} \Big|_{q=q_0}. \quad (32a,b)$$

By substituting Eqs. (31a,b) into Eqs. (29b,c) and making use of Eq. (14), we find formulas for the asymptotic (high wave number) growth rates:

$$s_1 = \lim_{\xi \rightarrow \pm\infty} \left[-\frac{f_u}{2} - \frac{1}{\lambda_{2\pm} - \lambda_{1\pm}} \left(h_0 f_h + \frac{B_1 f_u}{2} \right) \right], \quad (33a)$$

$$s_2 = \lim_{\xi \rightarrow \pm\infty} \left[-\frac{f_u}{2} + \frac{1}{\lambda_{2\pm} - \lambda_{1\pm}} \left(h_0 f_h + \frac{B_1 f_u}{2} \right) \right]. \quad (33b)$$

These expressions can become unbounded if $\lambda_{2\pm} - \lambda_{1\pm} \rightarrow 0$. This is a signature of ill-posedness within the initial value problem constructed in the linear stability analysis, which ultimately stems from loss of hyperbolicity when the characteristics of the governing equations coalesce [39]. While this is not possible within the classical shallow-water framework where $\beta(h, u) = 1$, it could occur for other choices of β . Specifically, from Eqs. (7) and (14), we see that $\lambda_1(h, u) = \lambda_2(h, u)$ if

$$hu^2 \frac{\partial \beta}{\partial h} = -\frac{1}{F^2} - u^2(\beta - 1) - \left[u(\beta - 1) + 2u^2 \frac{\partial \beta}{\partial u} \right]^2. \quad (34)$$

Increasing flow depth independently of other variables implies an increase in flow Reynolds number, leading (in general) to blunter vertical flow profiles, i.e., decreasing $\beta(h, u)$. Therefore, $\partial\beta/\partial h < 0$

is not unexpected and particular care should be taken to avoid choices of β that lead to an ill-posed model.

Traveling waves can become unstable if s_1 or s_2 crosses zero in either far-field limit. By rearranging either $s_1 = 0$ or $s_2 = 0$ we obtain the same expression for the value of F at which flow becomes unstable in these regions. The lesser of these two values is the ‘‘critical’’ F above which, linear instability of the traveling wave is guaranteed. In the special case $\beta(h, u) = 1$, we label this F_{Tr} and find that

$$F_{\text{Tr}}^2 = \min_{\ell=\pm\infty} \lim_{\xi \rightarrow \ell} \frac{f_u^2}{h_0 f_h^2}. \quad (35)$$

The square of the corresponding local Froude number is $F_{\text{Tr}}^2 u_0^2 / h_0$, where u_0 and h_0 in this instance are assumed to be evaluated in the relevant far-field limit. Regardless of which limit applies, this agrees (as it must) with the Froude number from Trowbridge’s stability criterion (2) for the linear stability threshold of a uniform shallow layer. In fact, since $u_0 \equiv u_0(h_0)$ and $\tau(\mathbf{q}_0) \rightarrow h_0$ as $|\xi| \rightarrow \infty$, we may differentiate with respect to h_0 to deduce that

$$\frac{f_h}{f_u} \rightarrow -\frac{du_0}{dh_0} \quad \text{as } |\xi| \rightarrow \infty. \quad (36)$$

Therefore, we obtain the slightly simpler and more intuitive formula

$$F_{\text{Tr}} = \min_{\ell=\pm\infty} \lim_{\xi \rightarrow \ell} \frac{1}{\sqrt{h_0} \left| \frac{du_0}{dh_0} \right|}, \quad (37)$$

which implies that the flow in the far fields is more unstable if the steady velocity is more sensitive to changes in the flow depth. As mentioned in the introduction, this extends a much older result of Craya [3] to the case of arbitrary drag (and monoclinal waves). While du_0/dh_0 is everywhere positive for most drag laws, the modulus signs in Eq. (37) are required in general. For example, confined channel geometries that narrow towards the top (such as partially wetted pipes) can lead to a turning point in $u_0(h_0)$ [40,41]. Some additional implications of Eq. (37) are given later in Sec. III B.

For general β , we shall write $F = F_c$ to denote the threshold of instability. As before, we rearrange either $s_1 = 0$ or $s_2 = 0$ to obtain an expression for F_c , which may be written in terms of F_{Tr} , as so

$$\frac{F_c^2}{F_{\text{Tr}}^2} = \min_{\ell=\pm\infty} \lim_{\xi \rightarrow \ell} \frac{1}{1 + \omega B_1 h_0^{1/2} F_{\text{Tr}} - B_2 F_{\text{Tr}}^2}, \quad \text{where } \omega = \text{sgn}(f_u/f_h). \quad (38)$$

Most typically, $\partial\tau(\mathbf{q}_0)/\partial h < 1$ and $\partial\tau(\mathbf{q}_0)/\partial u > 0$, implying that $f_u/f_h < 0$ (as originally assumed in Ref. [14]). Nevertheless, Eq. (38) accounts for choices of τ where these inequalities do not necessarily hold.

To illustrate the effect that the momentum shape factor can have on the critical F , we consider the case where β is approximated by a constant value. Moreover, we suppose that the value of F_c is dictated by the upstream regime and $\omega = -1$. (Both of these conditions are met in the cases of Chézy, granular, and viscous drag closures.) Then we Taylor expand Eq. (38) in powers of $(\beta - 1)$ to obtain

$$F_c^2 = F_{\text{Tr}}^2 + (\beta - 1)F_{\text{Tr}}^3(2 + F_{\text{Tr}}) + \dots \quad (39)$$

Therefore, increasing β raises the threshold for instability. Indeed, the denominator in Eq. (38) vanishes in this case, if

$$\beta = 1 + \frac{1}{F_{\text{Tr}}(F_{\text{Tr}} + 2)}, \quad (40)$$

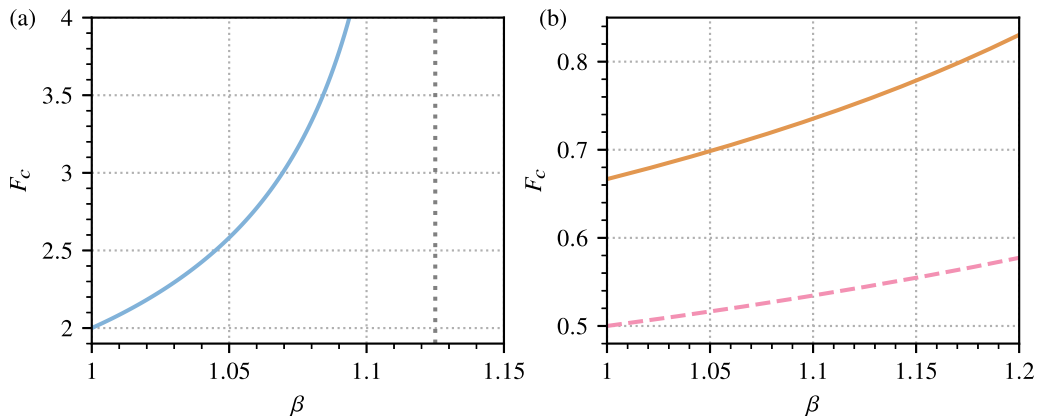


FIG. 7. Dependence of the critical $F = F_c$ for instability of traveling waves on a constant (h - and u -independent) momentum shape factor β for (a) Chézy drag and (b) granular (solid) and viscous (dashed) drag. In panel (a) the asymptote at $\beta = 1.125$ is also plotted (dotted).

with F_c becoming unbounded as β approaches this value. In Fig. 7 we plot $F_c(\beta)$ for our example drag closures. For Chézy drag [Fig. 7(a)], F_c increases rapidly with β and diverges at $\beta = 1.125$. The corresponding curves for granular and viscous drag [Fig. 7(b)] increase more steadily (though nevertheless significantly). The qualitative difference between the effect of β across the two panels is encapsulated by Eq. (39).

The stabilizing influence of larger $\beta > 1$ here may be explained within the inequality given in (30). It may be deduced in this case that instability occurs when the bulk disturbance wave speed in the upstream regime, a_- , surpasses the characteristic velocity λ_{2-} . Referring to Eqs. (14b) and (31b), we note that increasing the vertical shear of the flow raises the speed of the characteristic while leaving a_- unchanged. This allows waves to remain stable at higher F . More generally, the effect of $\beta(h, u)$ on the characteristics explains the modified stability threshold of Eq. (38).

B. Implications for different solution regimes

With the stability threshold determined, we may investigate which kinds of solution are stable or unstable. First, we examine the stability of continuous monoclinal waves versus shock solutions.

Inequality (30) allows us to prove an observation from Sec. II, that the regime boundaries demarcating the onset of shock development and existence of traveling wave solutions (see Fig. 4) must intersect at $(h_\infty, F) = (1, F_c)$. Recall that these boundaries are given by the lines $\lambda_{2+} = 0$ and $\lambda_{2-} = 0$ respectively. When $h_\infty = 1$, we compute $a_- = a_+ = 1 - c_0(1) - \lim_{|g| \rightarrow \infty} (f_h/f_u)$, where c_0 is written as a function of h_∞ , as in Sec. II. We deduce via Eq. (10), that $c_0(1) = 1 + (du_\infty/dh_\infty)|_{h_\infty=1}$. Therefore, by Eq. (36) we obtain $a_\pm = 0$. This implies, by inequality (30), that instability of the uniform layer occurs exactly when $\lambda_{2-} = \lambda_{2+} = 0$, i.e., the intersection point of the two traveling wave regime boundaries.

If the cases depicted in Fig. 4 (Chézy and granular drag) are no more unstable in the downstream direction than upstream, it follows that continuous monoclinal waves are always stable, because the curve bounding the onset of shock development ($\lambda_{2+} = 0$) is monotonic and bounded above by the stability threshold of upstream flow, $F = F_c(1)$. In the case of granular drag, we already observed in Fig. 6, that modes which are undamped upstream turn unstable at lower F_c than modes which are undamped downstream. More generally, if τ does not depend on any physical scales other than the flow height and velocity, the local Froude number at which the downstream regime becomes unstable must equal the critical Froude number of the upstream flow, $F_c(1)$. Since the local Froude number in the downstream region differs from that of the upstream region by a factor of $u_\infty/\sqrt{h_\infty}$,

we may write

$$F_c(h_\infty) = \min \{F_c(1), F_c(1)\sqrt{h_\infty/u_\infty}\}. \quad (41)$$

In this case, instability first occurs in the upstream flow if and only if $\sqrt{h_\infty}/u_\infty > 1$.

If additional physical scales are present in the drag formulation, then Eq. (41) cannot be used and the argument of Eq. (37) must be evaluated in both far-field regimes to determine which region is more vulnerable to instability. An example of a drag law that requires this treatment is given by the resistance of a turbulent fluid in an open rectangular channel of width w , which we nondimensionalize with respect to H , as in Eq. (4c). Assuming the Chézy formula for turbulent bottom drag, then $\tau = (w + 2h)u^2/(w + 2)$ (see, e.g., Refs. [41,42] for details on how to calculate such formulas). Then, in either far field, using $\tau(q_0) = h_0$, we compute $(\sqrt{h_0}du_0/dh_0)^{-1} = 2(w + 2h_0)\sqrt{h_0}/(u_0w)$. In the downstream direction, $h_\infty/u_\infty^2 = (w + 2h_\infty)/(w + 2)$, which is strictly less than one for $h_\infty < 1$. Therefore, the downstream limit dictates the evaluation of Eq. (37), and we determine the stability threshold

$$F_{\text{Tr}} = 2 \left(1 + \frac{2h_\infty}{w}\right) \sqrt{\frac{w + 2h_\infty}{w + 2}}. \quad (42)$$

Note that the correction in Eq. (38) may be applied, if necessary, to obtain the critical F for a general β . It is straightforwardly verified that this stability threshold could not have been obtained from Eq. (41). If $h_\infty = 1$, Eq. (42) agrees with the critical Froude number $F_{\text{Tr}} = 2(1 + 2/w)$ for uniform layers in a rectangular channel [16]. When $h_\infty < 1$, the effective channel breadth, measured with respect to the local flow height (i.e., w/h_0), is greater downstream than upstream. Therefore, since uniform layers in narrower channels are more stable, the downstream flow turns unstable at lower F , except in the limit $w \rightarrow \infty$, where $F_{\text{Tr}} \rightarrow 2$ and both regions turn unstable at the same F .

In the various cases where the drag law permits us to find a power law for the velocity of a steady layer, $u_0 = h_0^m$, Eq. (41) does apply, and it is straightforward to see that the upstream flow becomes unstable at lower F than the downstream flow if and only if $m > 1/2$. Here Eq. (37) implies the following strikingly simple formula for the linear stability threshold when $\beta(h, u) = 1$:

$$F_c = F_{\text{Tr}} = \min_{h_0=1, h_\infty} \frac{1}{|m|h_0^{m-1/2}}. \quad (43)$$

This result may be used to derive various well-known stability results, by selecting different m , e.g., for Chézy, granular and viscous uniform layers, $u_0 = h_0^{1/2}$, $h_0^{3/2}$, h_0^2 and $F_{\text{Tr}} = 2$, $2/3$, and $1/2$, respectively [1,6,14].

We can now address whether continuous monoclinal waves (with $\beta = 1$) are always stable in general for the class of drag laws with $u_0 = h_0^m$. The upper bound of the continuous solution regime ($\lambda_{2+} = 0$) may be rearranged to give the maximum F for continuous waves, $F = F_{\text{cont}}(h_\infty) = \sqrt{h_\infty(1 - h_\infty)}/(1 - h_\infty^m)$. This curve is strictly increasing for $m \leq 3/2$. It is straightforward to show in this case, using Eq. (43), that $F_{\text{cont}}(h_\infty) < F_c(h_\infty)$, regardless of whether $m < 1/2$. If instead, $m > 3/2$, then $F_{\text{cont}}(h_\infty)$ possesses a turning point, which lies within the interval $0 < h_\infty < 1$, for all $m > 2$. It is in this latter case only that continuous monoclinal waves can suffer linear instability without first developing a shock. An example of a system where continuous waves are not always stable is provided by the family of “power-law” fluids with drag formula $\tau(h, u) = (u/h)^n$, where $n > 0$ is a constant [10]. Then, $u_\infty(h_\infty) = h_\infty^{1+1/n}$, implying that there exist continuous power-law waves with $n < 1$ (within a suitable range of h_∞) that become unstable prior to shock development.

Using the same assumptions as above, we investigate the stability of upturned shock solutions (states with $h_0(0^-) > 1$). The critical case, where shocks are neither downturned nor upturned, is given by $h_0(0^-) = 0$. Consulting Eq. (13), we rearrange to obtain the curve

$$F = F_{\text{up}}(h_\infty) = \frac{(1 + h_\infty)^{1/2}(1 - h_\infty)}{(2h_\infty)^{1/2}(1 - h_\infty^m)}. \quad (44)$$

Above this value of F , solutions are upturned. We note, by L'Hôpital's rule, that F_{up} also passes through $F_c(1) = 1/m$ at $h_\infty = 1$. Moreover, assuming $m > 0$, we note that $F_{\text{up}}(h_\infty) \rightarrow \infty$ as $h_\infty \rightarrow 0^+$. The curve has a turning point within $0 < h_\infty < 1$ only if $m < 1/2$. Therefore, all upturned shocks with $m \geq 1/2$ are unstable. For $m < 1/2$, we must assess whether the existence of the turning point allows $F_{\text{up}}(h_\infty)$ to drop below $F_c(h_\infty)$ for any $0 < h_\infty < 1$. In Appendix A we show that it does not, and hence we conclude that upturned shock solutions are unstable for any m .

IV. EIGENMODE STRUCTURE

In addition to the linear growth rate, σ , the spatial structure of the corresponding modes plays a role in determining the evolution of disturbances. We saw in Figs. 5 and 6 that the modes for granular traveling waves are essentially oscillatory and can become dramatically amplified at the wave front in some cases. In this section, we demonstrate that this amplification occurs for generic choices of τ and show how it may be computed asymptotically when the wave number is large.

Since the dominant disturbances are purely harmonic in at least one of the far-field regions, we shall focus on modes which are undamped in the upstream direction, i.e., $k_- \in \mathbb{R}$. It is straightforward to adapt our analysis below to situations where the modes are undamped in the downstream. The regimes of high and low wave number present tractable opportunities to understand the spatial variation of modes. In the latter case, we note (as discussed in Sec. III) that the higher of the two branches of σ passes through $\sigma = 0$ when $k_- = 0$. By inspecting Eq. (21), it is immediately clear that an $O(\varepsilon)$ perturbation to σ away from zero, does not alter \hat{q}_1 to leading order. In other words, at low k_- , modes are asymptotically close to the neutral modes at $\sigma = 0$. This is evident, even in modes that are some distance from the origin of the spectral plane. For example, the darker curve in Fig. 5(e) clearly inherits its amplified peak at $\xi = 0$ from the corresponding neutral mode $\hat{q}_1 = (-h_0, -u_0)$, plotted in Fig. 5(b).

Therefore, we proceed to the high-wave number limit, $k_- \gg 1$, which we have shown above determines the most rapidly growing perturbations when the traveling wave is unstable. This is a richer problem, which we find necessary to divide into two cases, depending on the downstream depth.

A. Finite downstream depth ($0 < h_\infty < 1$)

First, suppose that the downstream height h_∞ is finite and nonzero. We analyze the spatial structure of \hat{q}_1 by employing a WKB approximation for the solution to Eq. (21) (see, e.g., Ref. [43] for details on this method). Setting $\varepsilon = 1/k_-$, we pose the ansatz

$$\hat{q}_1(\xi) = e^{i\phi(\xi)/\varepsilon} [\hat{r}_0(\xi) + \varepsilon \hat{r}_1(\xi) + \dots], \quad (45a)$$

$$\sigma = \varepsilon^{-1} \sigma_0 + \sigma_1 + \dots, \quad (45b)$$

in the regime $\varepsilon \ll 1$, where the unknown functions ϕ , \hat{r}_0 , \hat{r}_1 and the constants σ_0 , σ_1 are understood to be $O(1)$ with respect to ε .

The leading component of the growth rate in Eq. (45b) is purely imaginary and given by the system characteristics [Eq. (14)]. This is a fact straightforwardly verified by substituting our expansions into Eq. (21) and keeping only the leading $O(\varepsilon^{-1})$ terms, to obtain

$$(\phi'J - i\sigma_0 I) \hat{r}_0 = \mathbf{0}. \quad (46)$$

Therefore, $i\sigma_0/\phi'$ is an eigenvalue of the Jacobian, i.e., a characteristic. To match a purely harmonic disturbance upstream, we must impose $\phi \rightarrow \xi$ as $\xi \rightarrow -\infty$. Therefore, $i\sigma_0 = \lim_{\xi \rightarrow -\infty} \lambda_j$, for either $j = 1$ or 2 , and we deduce that

$$\phi'(\xi) = \frac{\lambda_j(1, 1)}{\lambda_j(h_0(\xi), u_0(\xi))}. \quad (47)$$

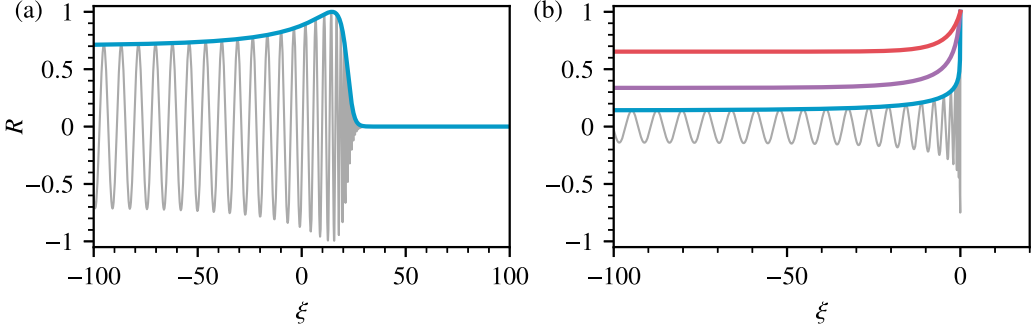


FIG. 8. Spatial variation of the mode amplitude function R , determined numerically via Eq. (52), for granular traveling waves with $h_\infty = 0.5$. (a) Amplitude $R(\xi)$ at $F = 0.5$ (blue), plotted alongside $u_1(\xi)$ (gray) for a spatially undamped mode with $\sigma = -0.014884 - i$. (This growth rate corresponds to $k_- \approx 0.74$. Higher wave number modes also agree well with R .) (b) Mode amplitudes for waves in the discontinuous traveling wave regime, for $F = 0.85$ (red), 0.7 (purple), and 0.55 (blue), approaching the critical $F \approx 0.547$, that marks the change between continuous and discontinuous states when $h_\infty = 0.5$ [see Fig. 4(b)]. The u_1 field for a corresponding mode in the $F = 0.55$ case, with $\sigma = -0.0113 - i$ ($k_- \approx 0.85$) is also plotted (gray).

This equation may be integrated (in principle) to obtain the frequency modulation of \hat{q}_1 , with respect to ξ . The only restriction on this procedure comes if the denominator in Eq. (47) vanishes. This occurs if one of the characteristics changes sign. As argued in Sec. II, only λ_2 can change sign along the wave and if it does so, this happens across a shock at $\xi = 0$. Therefore, provided the hydraulic jump has finite depth, λ_2 is nonzero either side of the shock.

The vector $\hat{r}_0(\xi)$ is given by the eigenspace for the characteristic curves as J varies along the slope. It may be neatly expressed using the characteristics themselves, as

$$\hat{r}_0(\xi) = R(\xi) \begin{pmatrix} 2h_0 \\ B_1 \pm (\lambda_2 - \lambda_1) \end{pmatrix}, \quad (48)$$

where $R(\xi)$ is an unknown amplitude that we aim to determine.

At $O(1)$, we find

$$(i\phi'J + \sigma_0 I)\hat{r}_1 = -J\hat{r}'_0 - (\sigma_1 I + N)\hat{r}_0. \quad (49)$$

To eliminate the unknown vector \hat{r}_1 , we appeal to the eigenproblem adjoint to Eq. (46),

$$\hat{l}_0^T (i\phi'J + \sigma_0 I)^T = \mathbf{0}, \quad (50)$$

and compute

$$\hat{l}_0(\xi) = L(\xi) \begin{pmatrix} 2(F^{-2} + B_2) \\ B_1 \pm (\lambda_2 - \lambda_1) \end{pmatrix}. \quad (51)$$

We are free to choose the amplitude function $L(\xi)$ and do so according to the constraint $\hat{l}_0 \cdot \hat{r}_0 = 1$. Then we project Eq. (49) onto \hat{l}_0 . By rearranging and setting $\bar{l}_0 = R\hat{l}_0$ and $\bar{r}_0 = R^{-1}\hat{r}_0$, we determine

$$\lambda_j \frac{R'}{R} = -\sigma_1 - \bar{l}_0 \cdot (J\bar{r}'_0 + N\bar{r}_0), \quad \text{for } j = 1, 2. \quad (52)$$

This is a first-order differential equation for the mode amplitude function R . Note that, as $\xi \rightarrow -\infty$, both $R' \rightarrow 0$ and $\bar{r}'_0 \rightarrow \mathbf{0}$, so $\sigma_1 = -\lim_{\xi \rightarrow -\infty} \bar{l}_0 \cdot N\bar{r}_0$. Since this expression is purely real, σ_1 must agree with the high wave number growth rate formulas already computed in Eqs. (33a,b). (Directly computing the matrix products confirms this.) In Fig. 8(a) we plot a numerical solution to Eq. (52) for granular drag with $F = 0.5$, $h_\infty = 0.5$. It accurately captures the amplitude

envelope of undamped eigenmodes, even those with modest far-field wave number ($k_- \approx 0.74$ in the plot).

When written in full, the final two terms of Eq. (52) are complicated analytical expressions, which depend on $q_0(\xi)$. Nevertheless, we can gain insight into the spatial variation of R by noting that away from the upstream far-field, the right-hand side must deviate from zero as the wave depth decreases (assuming $h_\infty < 1$). Therefore, if λ_j becomes small (compared with σ_1), we should expect to see $R(\xi)$ grow rapidly (and exponentially) from its far-field value in the region of the wave front. Moreover, Eq. (47) implies a corresponding rapid frequency change. There are two situations in which this can occur. First, in the case of discontinuous waves, λ_2 changes sign at the shock. Therefore, if the shock depth is shallow, λ_2 is necessarily small either side of $\xi = 0$ and becomes zero in the limit $h_0(0^-) \rightarrow h_\infty$. We saw the effect of this in Fig. 6(b), which shows an eigenmode for a wave that is very close to the regime boundary between continuous and discontinuous solutions. In Fig. 8(b), we plot $R(\xi)$ for $h_\infty = 0.5$ and $F = 0.85, 0.7, 0.55$. As F approaches the regime boundary at $F \approx 0.547$, $R(\xi)$ exhibits progressively greater amplification at the shock. The second situation where λ_2 can become small, leading to similar amplification, is in the limit $h_0, B_1 \rightarrow 0$, that is, as the traveling wave approaches a ‘‘flood wave’’ with dry downstream region. We consider the limiting case in the next section.

B. Flood waves ($h_\infty = 0$)

If $\beta(h, u) = 1$, flood waves suffer from a loss of strict hyperbolicity at the front, where (recalling that $u_0 = c_0 = 1$ in this case) their characteristics are identically zero. As argued in the previous subsection, this renders inappropriate the standard WKB ansatz in Eq. (45a). Here we provide a separate analysis for this typical special case, in which the underlying traveling wave equation (9) simplifies considerably to

$$h'_0 = F^2 \left[1 - \frac{\tau(h_0)}{h_0} \right]. \quad (53)$$

In the case of Chézy drag, a conceptually similar (though inequivalent) equation was solved analytically by Bresse, who sought stationary steady solutions to Eqs. (1a) and (1b) (i.e., $c_0 = 0$ and $u_0 = 1/h_0$) [44]. Bresse’s solution in terms of elementary functions is commonly available in hydraulics textbooks (see, e.g., Refs. [41,42]). For traveling flood waves ($c_0 = 1$), the profile differs. Specifically, we may integrate Eq. (53) with $\tau(h_0) = u_0^2 = 1$, to obtain $h_0(\xi) = W[-\exp(F^2\xi - 1)] + 1$, where W is Lambert’s function. Equation (53) has also been studied in the context of granular avalanches [22,23] and likewise admits an analytical solution [23].

A dry downstream region places some extra constraints on the linear stability formulation posed in Sec. III. The traveling wave velocity must equal the flow velocity at the front, so $c_1 = u_1(0^-)$. Furthermore, there can be no disturbance for $\xi > 0$, so $h_1(0^+) = u_1(0^+) = 0$. Finally, in order for the perturbation to be considered small in the front region, $h_1(0^-) = 0$, and we must check that $h_1 \lesssim h_0$ as $h_0 \rightarrow 0$.

Depending on the drag law, h_0 varies differently in the front region. We encompass these different profiles by writing the general expansion

$$\tau(h_0, u_0) = \Lambda(h_0, u_0)h_0^\delta + O(h_0^{\delta+1}), \quad (54)$$

where $\Lambda(h_0, u_0)$ is finite and nonvanishing as $h_0 \rightarrow 0$ and δ is an arbitrary exponent. For our three main example closures, $\delta = -1$ (viscous), $\delta = 0$ (Chézy), and $\delta = 1$ (granular). Substituting Eq. (54) into Eq. (53) and simplifying yields

$$h'_0 = F^2(1 - \Lambda h_0^{\delta-1}) + \dots \quad (55)$$

For any $\delta > 1$ the last term is subdominant at the front and the resulting equation leads to negative flow depths. Therefore, we discount these cases. Otherwise, Eq. (55) may be integrated to give

$$h_0 = (-A\xi)^\gamma + \dots \quad \text{when} \quad -1 \ll \xi < 0, \quad (56)$$

where $\gamma = 1/(2 - \delta)$ and

$$A = \begin{cases} (2 - \delta)F^2[\Lambda(0, 1) - 1] & \text{if } \delta = 1, \\ (2 - \delta)F^2\Lambda(0, 1) & \text{if } \delta < 1. \end{cases} \quad (57)$$

On substituting Eqs. (54) and (56) into the linear stability problem, Eq. (21), it may be deduced that h_1 is at most order $(-\xi)^\gamma$ at the front. The details are given in Appendix B. Therefore, $\varepsilon|h_1| \ll h_0$, for sufficiently small $\varepsilon > 0$, implying that solutions to Eq. (21) are indeed linear perturbations in the case of flood waves.

To capture the structure of these modes at high wave number, we employ a slightly modified version of Eqs. (45a,b). Since only one far-field direction is relevant for the linear flood wave problem, we shall write $k \equiv k_-$. At leading order in $\varepsilon = 1/k \ll 1$, we suppose

$$\hat{q}_1(\xi) = R(\xi)e^{i\phi(\xi)/\varepsilon}(\hat{r}_0 + \varepsilon\hat{r}_1 + \dots) + S(\xi)e^{-i\phi(\xi)/\varepsilon}(\hat{s}_0 + \varepsilon\hat{s}_1 + \dots), \quad (58a)$$

$$\sigma = \varepsilon^{-1}\sigma_0 + \sigma_1 + \dots, \quad (58b)$$

where $R(\xi)$ is finite and nonvanishing and $S(\xi)$ vanishes as $\xi \rightarrow -\infty$. The conjugate term in Eq. (58a) is necessary in this case to correctly represent the mode towards the front region—a point which will be clarified later. Linear independence of these terms means that the analysis to determine $\hat{r}_0, \hat{r}_1, \dots$ is identical to the presentation in Sec. IV A. However, as anticipated, evaluating Eq. (47) and integrating gives

$$\phi(\xi) = \int_0^\xi \frac{1}{\sqrt{h_0(s)}} ds, \quad (59)$$

meaning that ϕ can no longer be considered $O(1)$ with respect to ε . Nevertheless, this integral is guaranteed to converge, since $\gamma \leq 1$. Therefore, we are required only to modify our asymptotic expansion for $\hat{q}_1(\xi)$ close to the front. Proceeding with the WKB analysis, we determine via Eq. (52), that

$$\frac{R'}{R} = -\frac{2F^2 f_h h_0 + 3h'_0 \pm 2F(2\sigma_1 + f_u)\sqrt{h_0}}{4h_0}. \quad (60)$$

Since the mode amplitude is constant in the far field, we write $R \rightarrow R_-$ as $\xi \rightarrow -\infty$, where R_- is to be determined. On integrating Eq. (60), we find

$$R(\xi)h_0(\xi)^{3/4} = R_- \exp\left(-\frac{F^2}{2} \int_{-\infty}^\xi f_h \pm \frac{2\sigma_1 + f_u}{F\sqrt{h_0}} d\xi\right), \quad (61)$$

where σ_1, f_u, f_h and h_0 are understood to be integrated with respect to the dummy slope variable ξ . The integrand in Eq. (61) vanishes in the far field in order to satisfy the boundary condition there. (This may be separately confirmed by computing σ_1 .) Therefore, we appeal to the near-front expansions in Eqs. (54) and (56) and deduce that the dominant part of the integral is

$$\exp\left(-\frac{F^2}{2} \int_{-\infty}^\xi f_h d\xi\right) = \exp\left[\frac{1}{2} \int_{h_0}^1 \frac{h_0^{\delta-1}}{h_0 - \Lambda(h_0, 1)h_0^\delta} \left(\frac{\partial \Lambda}{\partial h_0} h_0 + (\delta - 1)\Lambda(h_0, 1)\right) dh_0\right] \sim h_0^{\frac{\delta}{2} - \frac{1}{2}} \quad (62)$$

to leading order. If $\delta = 1$, we must require that $\partial \Lambda / \partial h_0$ is nonzero. However, we can see from Eq. (55) that this is necessary for a front to form in the first place. Therefore, from Eq. (61), we deduce that $R(\xi) \sim h_0^{(2\delta-5)/4} = h_0^{-(2+\gamma)/(4\gamma)}$ at the front. Since $0 < \gamma \leq 1$, it diverges at least as rapidly as $h_0^{-3/4}$ there. Consequently, the WKB approximation cannot attain the boundary condition $(h_0, u_0) = (0, 1)$ at the front and as expected, we must consider this region separately.

To examine this inner region it is convenient to write the eigenmode equations (21) as a single second-order equation for u_1 . We obtain

$$h_0 u_1'' + (2h_0' + F^2 f_h h_0) u_1' - F^2 \sigma (\sigma + f_u) u_1 = 0. \quad (63)$$

By evaluating (59) near the front we note that $\phi \sim \varepsilon$ when $\xi \sim \varepsilon^{2/(2-\gamma)}$. Consequently we set $\eta = -\xi/\varepsilon^{2/(2-\gamma)}$ in order to capture this inner scale. We may write the spatial derivatives, $h_0, h'_0, f_h,$ and f_u in terms of η , once again making use of our expansions in Eqs. (54) and (56). On substituting these into Eq. (63) and making use of our expansion for σ in Eq. (58b) [note that $\sigma_0^2 = -1/F^2$ may be determined from Eqs. (46) and (47)], the leading part of the resulting equation is found to be $O(\varepsilon^{-2})$. It reads

$$\frac{d^2 u_1}{d\eta^2} + \frac{1+\gamma}{\eta} \frac{du_1}{d\eta} + \frac{1}{(A\eta)^\gamma} u_1 = 0. \quad (64)$$

The solution that passes through $u_1(0) = 1$ is given by

$$u_1(\eta) = \Gamma\left(\frac{2}{2-\gamma}\right) Y^{\gamma/(2-\gamma)} J_{\gamma/(2-\gamma)}(2Y), \quad (65)$$

where $Y = \eta(2-\gamma)^{-1}(A\eta)^{-\gamma/2}$, Γ is the gamma function and J_n denotes the Bessel function of the first kind of order n . In the far field $\eta \gg 1$, we find

$$u_1(\eta) \sim \frac{1}{\pi^{1/2}} \Gamma\left(\frac{2}{2-\gamma}\right) Y^{(\gamma+2)/(2\gamma-4)} \cos\left(2Y - \frac{(\gamma+2)\pi}{4(2-\gamma)}\right). \quad (66)$$

We note that $Y^{(\gamma+2)/(2\gamma-4)} \sim (-\xi)^{-(2+\gamma)/4} \sim h_0^{-(2+\gamma)/(4\gamma)}$, in agreement with the near-front scaling of the outer WKB approximation. Moreover, by substituting $h_0 = (-A\xi)^\gamma$ into Eq. (59) and integrating, it is straightforward to show that $2Y = \phi/\varepsilon$. Therefore, as η becomes large, the decaying oscillations of Eq. (65) match the leading-order behavior of the outer solution constructed in Eq. (58a) as ξ becomes small. It was for the purpose of matching the cosine function in Eq. (66) that we included the conjugate term in the WKB ansatz. However, since $S(\xi) \rightarrow 0$ as $\xi \rightarrow -\infty$, we concentrate on determining $R_- = \lim_{\xi \rightarrow -\infty} R(\xi)$. By appealing to Eqs. (61), (62), and (66), we establish that

$$|R_-| = \frac{[(2-\gamma)\varepsilon A]^{(\gamma+2)/(4-2\gamma)}}{2\pi^{1/2}} \Gamma\left(\frac{2}{2-\gamma}\right) \exp(\mathcal{I}), \quad (67)$$

where

$$\mathcal{I} = \int_0^1 \frac{F f_h h_0 \pm (2\sigma_1 + f_u) h_0^{1/2}}{2F(\tau_0 - h_0)} + \frac{(1-\gamma)}{2\gamma h_0} dh_0. \quad (68)$$

Equations (67) and (68) complete the matched expansion for marginal flood wave stability modes at high wave number $k = 1/\varepsilon$. Note that the two expressions for the integral in Eq. (68) correspond to two independent branches of modes with asymptotic growth rate $\sigma_1 = -\lim_{\xi \rightarrow -\infty} (f_u \pm F f_h)/2$, as determined by the formulas in Eqs. (33a,b) (or the analysis of Sec. IV A). The amplitude $|R_-|$ dictates the asymptotic decay of $u_1(\xi)$ in the far field, or equivalently, the growth of the perturbation at the front. Noting that $1/|R_-| \sim k^{(\gamma+2)/(4-2\gamma)}$ for $k \gg 1$, we see that disturbances ultimately become severely amplified from tail to front as $k \rightarrow \infty$, regardless of the drag formulation, since

$$k^{1/2} < k^{(\gamma+2)/(4-2\gamma)} \leq k^{3/2}. \quad (69)$$

In nature, this amplification is not truly unbounded, since we expect it to be ultimately damped by physical processes omitted from the governing equations that are only relevant at small length scales (e.g., turbulent diffusion). Nevertheless, this divergent behavior dictates the spatial properties of modes at finite, but large, wave number. For our example drag formulations, $1/|R_-| \sim k^{7/10}$ (viscous), $k^{5/6}$ (Chézy), and $k^{3/2}$ (granular). We verify the asymptotic formula of Eq. (67) numerically in Fig. 9, by plotting the far-field amplitude of $u_1(\xi)$ for the dominant (higher σ_1) branch of modes, over a range of k . This agrees well with $|R_-|$ as $k \rightarrow \infty$. The predicted scaling emerges early on, particularly in the granular case, where the modes have decayed to one tenth of their original amplitude by $k \approx 5$.

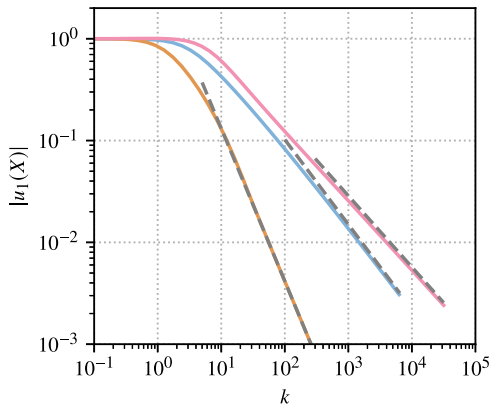


FIG. 9. Far-field amplitudes of (the dominant branch of) marginal eigenmodes, for $F = 2.5$ flood waves with (a) Chézy (blue), (b) granular (orange), and (c) viscous (pink) drag. For each drag law, we compute u_1 from Eq. (21) and evaluate its amplitude at $\xi = X = -40$, which (at the given F) is sufficiently far upslope that the underlying traveling wave approximates a uniform layer. Also plotted in each case is a section of the corresponding asymptotic amplitude $|R_-|$ (dashed gray), given by Eq. (67), verifying convergence as $k \rightarrow \infty$.

V. DISCUSSION

We have presented detailed analysis of the linear stability properties of monoclinal traveling waves in shallow flows of arbitrary rheology. By considering a setting that encompasses a broad family of flow models, the essential differences separating the properties of various flows are elucidated. In Table I we summarize some of our conclusions for different drag parametrizations, in the case where the momentum shape factor $\beta(h, u) = 1$. In addition to the example drag laws used throughout the paper, we include the properties of the general function $\tau(h, u) = u^a h^b$, where a and b are arbitrary constants. This parametrization encompasses Chézy, viscous, power-law drag and many other possible drag laws. Its listed properties may be readily determined using the results of Secs. III and IV.

As shown in Sec. III, the linear stability threshold for traveling waves is ultimately given by Trowbridge's criterion (2) applied to the upstream and downstream regions, plus a correction if β deviates from unity, given by Eqs. (38) and (39). The corresponding critical F (labeled F_{Tr}) is provided in the second column of Table I. The third column gives the dependence of the downstream velocity on the flow height. It highlights the simpler linear stability relationship, derived in Eq. (37), where F_{Tr} is given by the inverse of the exponent in the formula $u_\infty(h_\infty) = h_\infty^m$ and more generally,

TABLE I. Summary of the stability properties for different drag laws, in the case $\beta(h, u) = 1$.

Drag	F_{Tr}	$0 < h_\infty < 1$			$h_\infty = 0$	
		$u_\infty(h_\infty)$	Shock before instability?	Upstream unstable first?	Front scaling	$1/ R_- $
u^2	2	$h_\infty^{1/2}$	Yes	No ($u_\infty/\sqrt{h_\infty} = 1$) ^a	$(-\xi)^{1/2}$	$\sim k^{5/6}$
$\mu(h^{3/2}/u)h$	2/3	$h_\infty^{3/2}$	Yes	Yes	$(-\xi)$	$\sim k^{3/2}$
$(u/h)^n$	$n/(n+1)$	$h_\infty^{1+1/n}$	Iff $n > 1$	Yes ($n > 0$)	$(-\xi)^{1/(2+n)}$	$\sim k^{\frac{5+2n}{6+4n}}$
$u^a h^b$	$ a / 1-b $	$h_\infty^{(1-b)/a}$	Iff $2a + b > 1$	Iff $a/2 + b > 1$	$(-\xi)^{1/(2-b)}$	$\sim k^{\frac{5-2b}{6-4b}}$

^aAs indicated, in this case the upstream and downstream Froude numbers are identical. However, in Sec. III B, we showed that the downstream turns unstable first if this drag formulation is generalized to include the effect confining the flow within a finite rectangular channel.

by the derivative of the steady velocity of a uniform layer with respect to its depth, evaluated in the appropriate far-field limit. For the general drag $\tau(h, u) = u^a h^b$, the exponents $a \neq 0$, $b = 1$ are interesting to consider, since $F_{\text{Tr}} \rightarrow \infty$ as $b \rightarrow 1$. A physical interpretation of this situation comes from the paper of Trowbridge, who showed how to reformulate inequality (2) as an energy stability criterion [14]. When specialized to the present case, that analysis shows that the rate of total energy input to an infinitesimal disturbance from gravitational forcing is always exceeded by the corresponding rate of energy loss due to work done by bottom stresses and consequently, linear perturbations can only decay (regardless of F). Such a τ arises in the limit of the drag from a turbulent rectangular channel considered in Sec. III B, as the channel width tends to zero ($a = 2$, $b = 1$). This limit has a practical application in modeling the flow of turbulent gravity currents through densely packed obstacles such as vegetated areas [12,45], but the relevant shallow water linear stability problem has not previously received attention.

Our analysis of linear stability thresholds may be adapted straightforwardly for the case of purely downslope perturbations of two-dimensional traveling waves which are uniform along the perpendicular cross-slope direction. However, recent work proves that Trowbridge's criterion is violated for some rheologies when non-slope-aligned disturbances are accounted for [17]. Therefore, a fully two-dimensional extension of our results would require some care. Furthermore, as discussed in Sec. III, our analysis only strictly covers the stability with respect to modes within the continuously parametrized essential spectrum of the linear problem. Consequently, it may be the case for some drag formulations, that unstable isolated modes exist at lower F than predicted here. This is important to consider. For example, in thin-film flows over an inclined plane controlled by viscous and capillary processes, discrete modes can drive instability of the contact line [46]. While numerical techniques exist that could rule out this possibility for specific instances of our setting [37], obtaining general analytical results presents a far greater challenge. Nevertheless, recent studies rule out destabilization by discrete modes for Chézy solutions, ultimately leading to a proof that traveling waves with $F < 2$ are nonlinearly stable [27,28]. Therefore, there is reason to hope that these efforts could be extended for other drag laws, or even a general drag term.

Also of interest are results concerning the properties of traveling wave solutions. In Sec. II we derived the regime of existence for continuous waves and their degeneration into discontinuous states. In the cases of Chézy and granular drag, increasing F for continuous states always leads to formation of a shock, prior to development of linear instability. Later, in Sec. III B, a condition for the existence of unstable continuous solutions was obtained and is applied in Table I (column four).

Traveling waves turn linearly unstable as their eigenmodes cross into the positive half-plane (see Fig. 6). In Sec. III, various spectra for granular waves were computed numerically and it was observed that the onset of instability was dictated by the destabilization of modes that are only nonzero upstream ($\xi < 0$). The far-downstream region remains stable until F reaches a higher value. The respective vulnerability of the far-field regimes depends on their local Froude numbers and is thus easily determined (see also Sec. III B). Analogous criteria for other drag laws are summarized in column five of Table I.

We plotted many example eigenmodes throughout the paper. They typically possess the intriguing property that their spatial frequency varies between limiting values upstream and downstream. The dominantly growing modes within unstable regimes are spatially undamped in at least one of the far-field directions and have asymptotically high wave number. Consequently, we have analyzed in detail this special class of modes. In Sec. IV we derived equations for the variation of their amplitude and frequency in space. Both of these quantities are often strongly amplified near the front of the wave. Most pressingly, the mode amplitude diverges for waves at the boundary between continuous and discontinuous states, and for waves with zero depth downstream. The latter case seems particularly important, due to the physical significance of flood wave states and the fact that divergence occurs independently of F . In Sec. IV B we showed that the rate of this divergence as the wave number increases, depends on the spatial variation of the underlying traveling wave close to the front. Granular waves, whose depth varies linearly with ξ at the front, diverge the most severely. (Drag formulations that would lead to stronger divergence are unable to form steady flood

wave solutions.) Results for other example drag laws are summarized in the final two columns of Table I, and we note that the complete asymptotic dependence for an arbitrary drag law is developed in Sec. IV B. An interesting open question is: to what extent does the extreme amplification of linear modes affect the nonlinear development of instabilities? While it seems likely for any reasonable drag formulation that roll waves emerge within uniform depth regions, there is also the potential for the front to become disrupted and even for the wave to split in two. Our analysis suggests that granular waves might be particularly vulnerable to disruption.

Though our findings have typically been illustrated using examples with $\beta(h, u) = 1$, we have largely been able to present results for the case of a general momentum shape factor closure. Increasing β to a constant value above unity acts to stabilize traveling waves and can have a significant effect on the linear stability threshold. This has been noted before in the cases of Chézy [16] and power-law drag [10]. For example, raising β to 1.05 in a turbulent (Chézy) fluid increases F_c from 2 to roughly 2.6. This suggests that when high-fidelity calculations or simulations are called for, a suitable model for β should be employed. The effects that variation of β with h and u have are nontrivial to tease apart with generality. Nevertheless, we included the derivatives $\partial\beta/\partial h$ and $\partial\beta/\partial u$ in our analysis, since even simple formulas for β might introduce this dependency, e.g., if shear is modeled as a function of flow Reynolds number. When including these terms, we find that it is important to avoid situations where the system could lose hyperbolicity (leading to an ill-posed initial value problem), which occurs if Eq. (34) is satisfied. Otherwise, we expect the effects of β to be essentially quantitative (though nevertheless important). Varying β does not appear to greatly affect the character of the wave profiles, except in cases wherein (fixing all other parameters) it causes solutions to cross a regime boundary, e.g., by converting a continuous state into a shock (see Fig. 4). Moreover, we note that shear in the flow profile does not affect the fact of mode amplification near the front regions of certain waves, despite its necessary influence on the details of the linear problem. The precise effects of momentum shape factor closures in individual models and on the linear and nonlinear development of instabilities offer interesting avenues for future research.

ACKNOWLEDGMENTS

We thank D. Barkley, L. T. Jenkins, C. G. Johnson, J. C. Phillips, L. S. Tuckerman, and M. J. Woodhouse for valuable discussions. This research was supported by the Newton Fund Grant No. NE/S00274X/1 and the Royal Society Grant No. APX/R1/180148.

APPENDIX A: UPTURNED SHOCKS ARE ALWAYS UNSTABLE

In this Appendix, we show that $F_{\text{up}}(h_\infty) > F_c(h_\infty) = h_\infty^{1/2-m}/m$ for all $0 < h_\infty < 1$ and $m < 1/2$, given the assumptions $\beta(h, u) = 1$, $u_\infty = h_\infty^m$ and $m > 0$. This completes the argument of Sec. III B that upturned shock solutions are unstable in this case, regardless of the drag law. By consulting Eq. (44) and rearranging $F_{\text{up}}(h_\infty) > F_c(h_\infty)$, we note that it is equivalent to confirm that

$$G(h_\infty; m) = \frac{(1 - h_\infty)(1 + h_\infty)^{1/2}}{\sqrt{2}} - \frac{h_\infty^{1-m} - h_\infty}{m} > 0. \quad (\text{A1})$$

If $m = 1/2$, then

$$G(h_\infty; m) = (1 - h_\infty^{1/2})[(1 + h_\infty^{1/2})(1 + h_\infty)^{1/2} - 2\sqrt{2}h_\infty^{1/2}], \quad (\text{A2})$$

and it is straightforwardly shown, e.g., via analysis of the term within the square brackets, that this function is strictly positive for $0 < h_\infty < 1$. Furthermore, we compute the derivative

$$\frac{\partial G}{\partial m} = \frac{h_\infty}{m^2} \left[\frac{1}{h_\infty^m} (1 + m \log h_\infty) - 1 \right], \quad (\text{A3})$$

which has zeros only at $h_\infty = 0, 1$ and is strictly negative for $0 < h_\infty < 1$. Therefore, decreasing m from $1/2$, increases $G(h_\infty; m)$ for any such h_∞ , implying that inequality (A1) holds for any $m < 1/2$, as required.

APPENDIX B: FLOOD WAVE NEAR-FRONT PERTURBATIONS

In the special case of flood waves ($h_\infty = 0$) and $\beta = 1$, studied in Sec. IV B, it is necessary to check that \hat{q}_1 can legitimately be considered as a linear perturbation at the front, where $h_0 \rightarrow 0$.

Since $u_0 = c_0 = 1$ for flood waves, the matrices J and N [defined in Eqs. (6) and (23)] are greatly simplified. We compute

$$J = \begin{pmatrix} 0 & h_0 \\ F^{-2} & 0 \end{pmatrix} \quad \text{and} \quad N = \begin{pmatrix} 0 & h'_0 \\ f_h & f_u \end{pmatrix}. \quad (\text{B1})$$

By making use of the near-front of expansions in Eqs. (54) and (56), we may then write down the linear problem in the front region

$$-F^{-2}h'_1 = \left[(\delta - 1)\Lambda(\mathbf{q}_0) + (-A\xi)^\gamma \frac{\partial \Lambda}{\partial h} \Big|_{q=q_0} \right] (-A\xi)^{-1}h_1 + \left[\sigma + (-A\xi)^{\gamma-1} \frac{\partial \Lambda}{\partial u} \Big|_{q=q_0} \right] u_1 + \dots, \quad (\text{B2a})$$

$$-u'_1 = \sigma(-A\xi)^{-\gamma}h_1 + \gamma A(-A\xi)^{-1}(c_1 - u_1) + \dots. \quad (\text{B2b})$$

Then we use the fact that $0 < \gamma \leq 1$ (using $\delta \leq 1$ and the definition of γ from Sec. IV B) to deduce that the $\partial \Lambda / \partial h$ term of Eq. (B2a) is subdominant and may be neglected.

A suitable expansion for the perturbations that satisfies the front conditions $h_1(0^-) = 0$, $u_1(0^-) = c_1$, is

$$h_1 = K_1(-\xi)^{\alpha_1} + \dots, \quad u_1 = c_1 + K_2(-\xi)^{\alpha_2} + \dots, \quad (\text{B3})$$

where α_1 , α_2 , K_1 , and K_2 are constants to be determined. On substituting these into Eqs. (B2a,b) we immediately see that, for the remaining terms to balance at leading order, $\alpha_1 = \gamma$ and $\alpha_2 = 1$. Therefore, since $h_0 = (-A\xi)^\gamma + \dots$ at the front, this means that $h_1 \lesssim h_0$ in the front region, as required.

-
- [1] H. Jeffreys, The flow of water in an inclined channel of rectangular section, *London Edinburgh Dublin Philos. Mag. J. Sci.* **49**, 793 (1925).
- [2] R. F. Dressler, Mathematical solution of the problem of roll-waves in inclined open channels, *Commun. Pure Appl. Math.* **2**, 149 (1949).
- [3] A. Craya, The criterion for the possibility of roll-wave formation, in Gravity Waves, National Bureau of Standards Circular 521 (NBS, New York, 1952), pp. 141–151.
- [4] G. B. Whitham, *Linear and Nonlinear Waves* (John Wiley & Sons, 1974).
- [5] S. B. Savage and K. Hutter, The motion of a finite mass of granular material down a rough incline, *J. Fluid Mech.* **199**, 177 (1989).
- [6] Y. Forterre and O. Pouliquen, Long-surface-wave instability in dense granular flows, *J. Fluid Mech.* **486**, 21 (2003).
- [7] Y. Forterre and O. Pouliquen, Flows of dense granular media, *Annu. Rev. Fluid Mech.* **40**, 1 (2008).
- [8] C. Di Cristo, M. Iervolino, A. Vacca, and B. Zanuttigh, Roll-waves prediction in dense granular flows, *J. Hydrol.* **377**, 50 (2009).
- [9] J. M. N. T. Gray and A. N. Edwards, A depth-averaged $\mu(J)$ -rheology for shallow granular free-surface flows, *J. Fluid Mech.* **755**, 503 (2014).
- [10] C.-O. Ng and C. C. Mei, Roll waves on a shallow layer of mud modelled as a power-law fluid, *J. Fluid Mech.* **263**, 151 (1994).

- [11] K. Liu and C. C. Mei, Roll waves on a layer of a muddy fluid flowing down a gentle slope—A Bingham model, *Phys. Fluids* **6**, 2577 (1994).
- [12] L. Hatcher, A. J. Hogg, and A. W. Woods, The effects of drag on turbulent gravity currents, *J. Fluid Mech.* **416**, 297 (2000).
- [13] A. J. Hogg and A. W. Woods, The transition from inertia- to bottom-drag-dominated motion of turbulent gravity currents, *J. Fluid Mech.* **449**, 201 (2001).
- [14] J. H. Trowbridge, Instability of concentrated free surface flows, *J. Geophys. Res.* **92**, 9523 (1987).
- [15] J. Langham, M. J. Woodhouse, A. J. Hogg, and J. C. Phillips, Linear stability of shallow morphodynamic flows, *J. Fluid Mech.* **916**, A31 (2021).
- [16] J. E. Berlamont and N. Vanderstappen, Unstable turbulent flow in open channels, *J. Hydr. Div.* **107**, 427 (1981).
- [17] J. Zayko and M. Eglit, Stability of downslope flows to two-dimensional perturbations, *Phys. Fluids* **31**, 086601 (2019).
- [18] M. J. Lighthill and G. B. Whitham, On kinematic waves I. Flood movement in long rivers, *Proc. R. Soc. London A* **229**, 281 (1955).
- [19] H. E. Jobson, Predicting river travel time from hydraulic characteristics, *J. Hydraul. Eng.* **127**, 911 (2001).
- [20] M. G. Ferrick, Simple wave and monoclinal wave models: River flow surge applications and implications, *Water Resour. Res.* **41**, W11402 (2005).
- [21] M. L. Shome and P. M. Steffler, Flood plain filling by a monoclinal flood wave, *J. Hydraul. Eng.* **132**, 529 (2006).
- [22] O. Pouliquen, On the shape of granular fronts down rough inclined planes, *Phys. Fluids* **11**, 1956 (1999).
- [23] J. M. N. T. Gray and C. Ancey, Segregation, recirculation and deposition of coarse particles near two-dimensional avalanche fronts, *J. Fluid Mech.* **629**, 387 (2009).
- [24] D. Razis, G. Kanellopoulos, and K. van der Weele, The granular monoclinal wave, *J. Fluid Mech.* **843**, 810 (2018).
- [25] D. Razis, G. Kanellopoulos, and K. van der Weele, A dynamical systems view of granular flow: From monoclinal flood waves to roll waves, *J. Fluid Mech.* **869**, 143 (2019).
- [26] G. Kanellopoulos, The granular monoclinal wave: A dynamical systems survey, *J. Fluid Mech.* **921**, A6 (2021).
- [27] Z. Yang and K. Zumbrun, Stability of hydraulic shock profiles, *Arch. Ration. Mech. Anal.* **235**, 195 (2020).
- [28] A. Sukhtayev, Z. Yang, and K. Zumbrun, Spectral stability of hydraulic shock profiles, *Physica D* **405**, 132360 (2020).
- [29] A. J. Hogg and D. Pritchard, The effects of hydraulic resistance on dam-break and other shallow inertial flows, *J. Fluid Mech.* **501**, 179 (2004).
- [30] W. C. Reynolds and W. G. Tiederman, Stability of turbulent channel flow, with application to Malkus's theory, *J. Fluid Mech.* **27**, 253 (1967).
- [31] R. S. Johnson, Shallow water waves on a viscous fluid—The undular bore, *Phys. Fluids* **15**, 1693 (1972).
- [32] O. Pouliquen and Y. Forterre, Friction law for dense granular flows: Application to the motion of a mass down a rough inclined plane, *J. Fluid Mech.* **453**, 133 (2002).
- [33] P. Jop, Y. Forterre, and O. Pouliquen, Crucial role of sidewalls in granular surface flows: Consequences for the rheology, *J. Fluid Mech.* **541**, 167 (2005).
- [34] P. Jop, Y. Forterre, and O. Pouliquen, A constitutive law for dense granular flows, *Nature (London)* **441**, 727 (2006).
- [35] O. Pouliquen, Scaling laws in granular flows down rough inclined planes, *Phys. Fluids* **11**, 542 (1999).
- [36] A. N. Edwards, A. S. Russell, C. G. Johnson, and J. M. N. T. Gray, Frictional hysteresis and particle deposition in granular free-surface flows, *J. Fluid Mech.* **875**, 1058 (2019).
- [37] B. Barker, J. Humpherys, G. Lyng, and J. Lytle, Evans function computation for the stability of travelling waves, *P. Roy. Soc. Lond. A. Mat.* **376**, 20170184 (2018).
- [38] G. B. Whitham, Some comments on wave propagation and shock wave structure with application to magnetohydrodynamics, *Commun. Pure Appl. Math.* **12**, 113 (1959).

- [39] D. D. Joseph and J. C. Saut, Short-wave instabilities and ill-posed initial-value problems, *Theor. Comput. Fluid Dyn.* **1**, 191 (1990).
- [40] T. R. Camp, Design of sewers to facilitate flow, *Sewage Works J.* **18**, 3 (1946).
- [41] V. T. Chow, *Open-Channel Hydraulics* (McGraw-Hill, New York, 1959).
- [42] F. M. Henderson, *Open Channel Flow* (Macmillan, New York, 1966).
- [43] C. M. Bender and S. A. Orszag, *Advanced Mathematical Methods for Scientists and Engineers* (McGraw-Hill, New York, 1978).
- [44] J. A. C. Bresse, *Cours De Mécanique Appliquée: Résistance Des Matériaux et Stabilité Des Constructions*, Vol. 1 (Mallet-Bachelier, Paris, 1859).
- [45] H. M. Nepf, Flow and transport in regions with aquatic vegetation, *Annu. Rev. Fluid Mech.* **44**, 123 (2012).
- [46] Y. Ye and H.-C. Chang, A spectral theory for fingering on a prewetted plane, *Phys. Fluids* **11**, 2494 (1999).